Maturation stage-specific V-ATPase disassembly can explain neutral pH of lysosome-related organelles

Ajay Pradhan[1,2] Niraj Tadasare[1] Debolina Sarkar[1,2] Vandna Maurya[1,2] Lavan K. Bansal[1] Aaron P. Turkewitz [3] Santosh Kumar [1,2,4 *]

[1]National Centre for Cell Science, NCCS Complex, Savitribai Phule Pune University Campus, Ganeshkhind Road, Pune 411007 Maharashtra, India
[2]Regional Centre for Biotechnology, NCR Biotech Science Cluster, Faridabad 121001 Haryana, India
[3]Department of Molecular Genetics and Cell Biology, The University of Chicago, Chicago IL USA 60637

[4]Lead contact
*Correspondence: sbalot@nccs.res.in, sbalot@gmail.com (S.K.)

Abstract
Lysosome-related organelles (LROs) are a heterogeneous family of organelles found in many cell types, whose significant similarities to lysosomes include their acidification by vacuolar-type ATPases (V-ATPases). However, some organelles with hallmarks of LROs are nonetheless non-acidic. Here we investigate this poorly understood phenomenon using the ciliate *Tetrahymena thermophila*, which have prominent secretory LROs called mucocysts. Using three different approaches, we show that mature mucocysts, poised for exocytosis, are non-acidic. Nonetheless, a specific V-ATPase a-subunit is targeted to mucocysts and is indispensable for mucocyst biogenesis and secretion. Consistent with this, immature mucocysts in the cytoplasm appear to be transiently acidified. The stage specificity of acidification can be explained by our finding that several canonical V-ATPase subunits are present in the immature, but not mature, mucocysts. Our data argue that a mucocyst-specific V-ATPase complex is targeted to newly-forming mucocysts and subsequently disassembles at a late stage in *Tetrahymena* LRO maturation, and that this depends on the AP-3 trafficking adaptor.

Introduction:
LROs, which include mammalian Weibel-Palade bodies, melanosomes, acrosomes, basophil granules, Lamellar bodies, and platelet-dense granules, are a family of organelles whose morphological and functional diversity belies that fact that they commonly depend on a set of highly conserved proteins for their biosynthesis (Delevoye et al., 2019; Khawar et al., 2019; Le et al., 2021; Marks et al., 2013; McCormack et al., 2017; Metcalf et al., 2008; Weaver et al., 2002). Though sharing features with both late endosomes and lysosomes, LROs are functionally, morphologically, and/or compositionally distinct (Luzio et al., 2014; Huizing et al., 2008; Marks et al., 2013). They are formed by a multistep process in which an immature organelle matures by acquiring cargo from both secretory pathways as well as traffic from endosomes (Bonifacino, 2004; EC et al., 2000; Raposo et al., 2007). Many of the protein cargoes targeted to LROs within the endomembrane network rely on receptors and cytoplasmic adaptors for their selection as well as complexes to tether and fuse vesicles (Banushi and Simpson, 2022; Marks et al., 2013). These include the AP-3 adaptor, the homotypic fusion and protein sorting (HOPS) complex, the small GTPases Rab32 and Rab38, the sorting receptor sortilin/VPS10, and three biogenesis of LROs (BLOC) complexes (Banushi and Simpson, 2022; Raposo et al., 2007; Marks et al., 2013; Gautam et al., 2006; Hermey, 2009; Starcevic et

al., 2002; Wasmeier et al., 2006; Kaur et al., 2017). Phylogenetic analysis of LRO machinery revealed that these LRO components were present in the last eukaryotic common ancestor (LECA) and a basic element of eukaryotic membrane trafficking (More et al., 2024).

One cargo broadly shared among LROs is the Vacuolar-type proton ATPase (V-ATPase) complex, whose presence drives acidification of the LRO lumen. Acidification plays a critical role for many types of LROs (EC et al., 2000; Pejler et al., 2017; Matsumoto and Nakanishi-Matsui, 2019; Sun-Wada et al., 2003). For instance, T lymphocytes and natural killer cells synthesise LROs called lytic granules, that maintain an acidic pH essential for the targeted release of macromolecules to eliminate virally-infected or tumor cells (Griffiths and Argon, 1995). Type II alveolar epithelial cells synthesise lamellar bodies that store lung surfactant. The processing and therefore release of surfactant proteins from lamellar bodies requires an acidic pH (Weaver et al., 2002; Chander et al., 1986; Chintagari et al., 2010). Sperm cells synthesize the acrosome, which contains various hydrolytic enzymes that are secreted to help the sperm in penetrating the egg's protective layers. An acidic environment is essential for the biogenesis and exocytosis of the acrosome (Berruti and Paiardi, 2011). In endothelial cells, Weibel-Palade bodies are formed from the trans-Golgi network (TGN) and mature into elongated, cigar-like structures that store the adhesive glycoprotein von Willebrand factor (VWF). This glycoprotein is essential for facilitating interactions between platelets and the vascular wall. The luminal acidification of Weibel-Palade bodies is a key factor for the dense packing of VWF and its release from endothelial cells (Naß et al., 2021).

V-ATPases are well-studied complexes that are composed of two macromolecular domains, V_1 and V_0. V_1, the catalytic domain, is a 650-kDa peripheral complex comprised of $A_3B_3CDE_3FG_3H$ subunits, that hydrolyzes ATP to generate the energy required for pumping protons (Forgac, 2007; Futai et al., 2019; Breton and Brown, 2013). V_0 is a 260-kDa integral membrane protein complex that forms a proton channel; it consists of $ac_8c'c''def$ subunits (Breton and Brown, 2013; Forgac, 2007; Futai et al., 2019). Thus, both the V_1 and V_0 subunits are required to form a fully functional holo-V-ATPase complex. Since V-ATPases are active in diverse intracellular compartments, compartment-specific stimulation of assembly or disassembly may be one organizing principle of the endomembrane network. For example, increasing assembly has been proposed as a cause of increased acidity throughout the endocytic route in mammalian cells (Lafourcade et al., 2008). Positive regulators of V-ATPase complex assembly include the heterotrimeric chaperone complex "RAVE (Regulator of ATPases of Vacuolar and Endosomal membranes)" as well as glycolytic enzymes phosphofructokinase-I and aldolase (Parra and Kane, 1998; Xu and Forgac, 2001; Lu et al., 2007; Chan and Parra, 2014; Smardon et al., 2015). Conversely, the complex's enzymatic activity can be downregulated by disassembly, in which the V_1 domain separates from the membrane-integral V_0 domain (Parra et al., 2014; Oot et al., 2017). In yeast and mammalian cells, reversible V-ATPase assembly and disassembly have been reported in response to stimuli including glucose and amino acid starvation and refeeding, and oxidative stress (Chan and Parra, 2014; Trombetta et al., 2003; Sautin et al., 2005; Stransky and Forgac, 2015; Bodzęta et al., 2017; Parra and Kane, 1998; Khan et al., 2022).

In addition to compartment-specific assembly/disassembly, V-ATPase activities in endocytic and secretory pathways can be tailored for different compartments based on the expression of multiple paralogs for some subunits (Toei et al., 2010). These paralogs have historically been called isoforms in the field, a terminology we will therefore adopt in this Introduction. Such isoforms can, among other things, provide determinants for compartment-specific targeting. In yeast, subunit-a has two isoforms, encoded by the *VPH1* and *STV1* genes

(Manolson et al., 1994, 1992). V-ATPases containing these alternate a-subunits differ in proton pump energy-coupling efficiency, subcellular localization, and in the regulation of subunit association under cellular metabolic conditions (Kawasaki-Nishi et al., 2001; Manolson et al., 1994). In mammals, most V-ATPase subunits exist in multiple isoforms that are expressed in a tissue-specific manner, and isoform-specific activities or localization have been demonstrated in many species (Toei et al., 2010; Breton and Brown, 2013; Forgac, 2007; Chu et al., 2021). For example, there are four subunit-a isoforms (a1-a4) which direct their cognate complexes to distinct cellular destinations (Sun-Wada and Wada, 2013; Chen et al., 2024; Matsumoto et al., 2018; Toei et al., 2010; Sun-Wada and Wada, 2022; Sun-Wada et al., 2007). Isoforms a1, a2, and a3 are associated with coated vesicles, the Golgi apparatus/early endosomes, and late endosomes/lysosomes, respectively (Breton and Brown, 2013; Chu et al., 2021; Toei et al., 2010). Subunit a3 in pancreatic islet cells also localizes to insulin granules, which are LROs whose maturation requires luminal acidification (Sun-Wada et al., 2006). An extreme example of such isoform-specific targeting comes from the ciliate *Paramecium tetraurelia,* in which seventeen a-subunit isoforms localize to at least seven different compartments (Wassmer et al., 2006). Compartment-specific isoforms are also known to play additional roles. For example, mammalian a3 is a determinant for Rab7-dependent trafficking of LRO proteins in osteoclasts (Matsumoto et al., 2018, 2022; Nakanishi-Matsui et al., 2024). Notwithstanding the importance of compartment-specific optimization, the conserved activity of V-ATPases is proton pumping. However, several recent studies have identified non-acidic and nondegradative LROs across different cell types, including melanocytes and neurons, as well as in unicellular eukaryotes such as *Dictyostelium* (Padh et al., 1993; Fok et al., 1993; Cheng et al., 2018; Hurbain et al., 2018; Correia et al., 2018; Yap et al., 2018). For example, LROs in melanocytes called melanosomes are only transiently acidic: premelanosomes are acidic, whereas mature melanosomes are non-acidic, which may be more consistent with their role as storage rather than degradative compartments (Hurbain et al., 2018; Correia et al., 2018; Le et al., 2021). A similar cellular logic may underlie the LAMP1-positive but non-acidic and non-degradative (i.e., lacking acid hydrolases) endolysosome-related organelles (ELROs) organelles found in neuronal cells (Cheng et al., 2018; Yap et al., 2018). In *Dictyostelium discoideum*, LROs called post-lysosomes originate as acidic lysosomes but subsequently lose their acidity and mature into neutral pH organelles (Padh et al., 1993; Fok et al., 1993). The mechanisms involved in the neutralization of these organelles in widespread eukaryotic lineages are not known.

One organism with non-acidic LROs is the ciliate *Paramecium tetraurelia*, where secretory LROs called trichocysts dock at the plasma membrane to release their contents via regulated exocytosis in response to extracellular stimuli (Plattner, 2017; Lumpert et al., 1992; de Loubresse et al., 1994). However, V-ATPase activity nonetheless appears required for trichocyst formation. To understand this paradox and shed light on the nature of neutral pH LROs, we have extended the analysis in *Paramecium* using the related Oligohymenophorean ciliate *Tetrahymena thermophila*, where the homologous organelles to trichocysts are known as mucocysts (Turkewitz, 2004). These have been characterized as LROs based on multiple lines of molecular evidence. Mucocysts, like LROs in many organisms, undergo biochemical and morphological maturation (Briguglio et al., 2013; Kumar et al., 2014, 2015; Kaur et al., 2017; Sparvoli et al., 2018). The most abundant mucocyst cargo proteins are encoded by two multigene families: *GRL* (granule lattice) and *GRT/IGR* (granule tip/induced on granule regeneration) (Bowman et al., 2005; Cowan et al., 2005; BOWMAN et al., 2005). Grls are synthesized as proproteins and subsequently cleaved and trimmed by processing enzymes Cth3p (Cathepsin 3) and Cth4p to generate mature Grls (Kumar et al., 2015, 2014). Mature Grls assemble to form a crystal that fills the mucocyst lumen and expands upon exocytic fusion

of a docked mucocyst, propelling the contents out to the extracellular space (Cowan et al., 2005). Grt/Igr proteins are not required for crystal formation or for content propulsion, and at least some family members are sub-localized within the mucocyst lumen (BOWMAN et al., 2005).

Importantly, cargo delivery to mucocysts involves at least two different pathways. The delivery of Cth3p and Grt/Igrs, but not Grls, requires the sortilin/VPS10 receptor Sor4p and an endosomal SNARE, Stx7l1p (Syntaxin 7-like) (Briguglio et al., 2013; Kaur et al., 2017; Sparvoli et al., 2018). The Grl and Grt proteins localize to different vesicles during mucocyst formation; these and other data argue that heterotypic fusion between secretory and endosomal vesicles is a key step in formation of ciliate LROs, like in other lineages. In *Tetrahymena* that fusion requires VPS8a, a subunit of a dedicated CORVET (class C core endosomal vacuole tethering) complex (Sparvoli et al., 2018). The formation of mucocysts also requires the AP3 complex, and cells lacking the AP3µ subunit accumulate abortive mucocyst intermediates distinct from those in *VPS8A* knockout cells (Kaur et al., 2017). However, the presumed AP3-dependent mucocyst cargo is not known.

In this study, we confirmed that mature mucocysts are not acidified. Nonetheless, their biogenesis and more specifically maturation depends on the V-ATPase a1-subunit isoform, one of six a-subunit paralogs/isoforms in this species, and which is localized to both immature cytoplasmic mucocysts as well as mature docked mucocysts. By targeting a pH-sensor to the mucocyst lumen, we found evidence the immature mucocysts are transiently acidified. Consistent with this, we found that other subunits of the V-ATPase are also present at that stage in mucocyst formation. Analysis of cells lacking a1-subunit expression suggests that the failure to acidify during mucocyst maturation leads to predictable defects in proprotein (Grl) processing, but also defects in the heterotypic vesicle fusion characteristic of LRO formation. In striking contrast, several other V-ATPase subunits are absent from mature docked mucocysts. Our findings suggest that the V-ATPase complex disassembles during mucocyst maturation, and can therefore account for the neutral pH of the mature organelles. In cells lacking AP3µ, the accumulated mucocyst intermediates appear to retain the full cohort of V-ATPase subunits, indicating that the activity of AP3 is required for V-ATPase disassembly.

Results

Expression profiling reveals co-regulation of mucocyst-associated proteins and V-ATPase-a1 subunit of the V_0 domain of V-ATPase complex in *T. thermophila*

The *T. thermophila* macronuclear genome has more than 24,000 predicted genes, including 11 that encode the subunits of the V_1 domain and 12 that encode the subunits of the V_0 domain of the V-ATPase complex (Coyne et al., 2008; Eisen et al., 2006). To ask whether there might be paralog-encoded subunits specialized for mucocysts, we followed up on earlier findings that many genes encoding mucocyst-related proteins are highly coregulated under a variety of conditions (Xiong et al., 2013; Briguglio et al., 2013; Kumar et al., 2014; Miao et al., 2009; Xiong et al., 2011). We used the online tools at the Tetrahymena Functional Genomics Database (http://tfgd.ihb.ac.cn/) to identify V-ATPase subunits that are coregulated with known mucocyst-associated genes. This search revealed that TTHERM_01332070, encoding an a-subunit of V-ATPase V_0, was coregulated with known mucocyst-associated genes **(Figure 1A)** and therefore represented a strong candidate for a mucocyst-specific V-ATPase subunit. We have given this paralog the name a1. In addition to TTHERM_01332070, the *T. thermophila* genome contains five additional paralogs, which we named *a2* (TTHERM_00463420), *a3* (TTHERM_00266570), *a4* (TTHERM_00372530), *a5* (TTHERM_01005210) and *a6* (TTHERM_01014710). These paralogs are significantly diverged, with a maximum of 45% amino acid sequence identity to the a1 paralog **(Figure S1)**, and they show transcriptional profiles distinct from that of a1 **(Figure 1B)**, consistent with the idea that they belong to complexes specialized for other cellular compartments.

Tetrahymena V-ATPase-a1p (where "p" denotes the protein) shares ~30% sequence identity with human subunit-a isoforms (a1p: ATP6V0A1, a2p: ATP6V0A2, a3p: ATP6V0A3 and a4p: ATP6V0A4). The predicted structure of the *T. thermophila* V-ATPase-a1p was strikingly similar to those of V-ATPase-a subunits in other lineages (shown for Opisthokonts) with 100% confidence and 85% coverage **(Figure 1C).** Structures similar to the *T. thermophila* V-ATPase-a1p (green) in the AlphaFold Protein Structure Database included the homologous a-subunits from *Saccharomyces cerevisiae* (yellow; A0A7I9G792) and *Mus musculus* (red; Q9Z1G4), the former with an 84% per-residue model confidence score (pLDDT) **(Figure 1D-E)**. The phylogenetic mapping of the a-subunits in *Tetrahymena* and in other organisms is consistent with the results of the structural analysis **(Figure S2)**.

V-ATPase-a1p localizes to mucocysts

To ask whether the *Tetrahymena* a1 subunit, implied via coregulation to be associated with mucocysts, is physically associated with this compartment, we tagged the protein via C-terminal fusion of the endogenous gene with 2 x mNeon. The expression in *Tetrahymena* of a fusion protein of the expected size was confirmed by immunoprecipitation followed by Western blotting **(Figure 2A)**. The localization of the fluorescent protein was examined by confocal microscopy and compared with mucocyst markers. In live cells, V-ATPase-a1p localized to linear arrays of fluorescent puncta at the cell surface, consistent with its accumulation in mucocysts **(Figure 2B, left panel, inset and Movie S1)**. In cross sections of the same cells, docked mucocysts are seen as elongated vesicles **(Figure 2B, right panel, inset and Movie S1)**. In addition, a significant fraction of V-ATPase-a1p localizes to heterogeneous cytoplasmic puncta at some distance from the cortex (which we call "non-cortical"). Approximately 75% of V-ATPase-a1p is present in the non-cortical compartments, with the remaining quarter located at the cell cortex in the docked mucocysts (**Figure 2C-D**).
Localization of a1p to mucocysts was confirmed by expressing tagged a1p in cells co-expressing mCherry-tagged mucocyst protein Grl3p. The two proteins showed strong co-localization (Manders' Coefficients 0.78± SD 0.10) in the docked mature mucocysts at the cell cortex **(Figure 2E, inset and 2F, left)**. In optical cross sections of the same cells, more limited overlap (Manders' Coefficients 0.26± SD 0.14) between a1p and Grl3p was observed, corresponding to overlap in non-cortical structures (**Figure 2E, Ei inset and 2F, right)**. We interpret non-cortical structures containing Grl3p as likely vesicular intermediates in mucocyst biogenesis.

Our results also indicate that a large fraction of non-cortical a1p is associated with compartments that do not also contain Grl3p. We found that non-cortical a1p showed significant overlap with the endocytic tracer FM4-64 (Manders' Coefficients 0.36± SD 0.12) (**Figure 2G-I**) and lesser overlap with the late endosomal marker Rab7p (Manders' Coefficients 0.17± SD 0.04) **(Figure S3A-C)** or with Lysotracker (Manders' Coefficients 0.08± SD 0.04) **(Figure S3D-F)**. Collectively, the findings support the idea that non-cortical V-ATPase-a1p is associated with biosynthetic mucocyst intermediates, and with endosomes that may be primarily be considered early or recycling.

Since other V-ATPase-a1 paralogs in *T. thermophila* show very different transcriptional profiles, we predicted that they would also reside in different compartments from a1. To examine this, we analyzed the localization of V-ATPase-a2p. This protein was found to be localized mostly near the plasma membrane but not co-localized with the mucocyst marker Grl3p **(Figure S3G)**.

Mucocysts are not stably acidic in *Tetrahymena*

Paramecium trichocysts which are homologous to *Tetrahymena* mucocysts, are not detectibly acidic (de Loubresse et al., 1994; Lumpert et al., 1992). However, in *Tetrahymena* mucocysts the key protease responsible for proGrl cleavage, called Cth3p, is related to lysosomal enzymes

(Kumar et al., 2014), and expected to be most active under acidic conditions. Therefore, we asked whether mucocysts maintained acidic luminal conditions. First, we incubated cells expressing Igr1p-mCherry with Acridine orange (AO) dye, which accumulates in acidic vesicles. There was no visible accumulation of AO at docked mature mucocysts **(Figure 3A)**. Similarly, we incubated cells expressing Grl3p-mCherry with an alternative probe for acidic compartments, Protonex Green (Prakash et al., 2021). Consistent with the AO results, we observed no concentration of Protonex Green in mature mucocysts at the cell cortex **(Figure 3B)**.

Given the significance of these data for interpreting the role of V-ATPase-a1, we took a third and more flexible approach to analyzing the pH of mucocysts by endogenously tagging Grl3p with either mEGFP or the super ecliptic pHluorin (SEP) variant, a green fluorescent protein whose emission is relatively quenched at acidic pH. In mammalian cells in which SEP is targeted to the lumen of acidified secretory vesicles, SEP emits bright fluorescence only after the vesicles undergo exocytosis, when their contents become neutralized (Benčina, 2013; Martinière et al., 2013; Michaluk and Rusakov, 2022). In our experiments, the salient advantage to using tagged Grl3p as a pH sensor is that it also allowed us to analyze the pH in the lumen of non-docked, immature mucocysts.

We first confirmed the expression of the fusion proteins Grl3p-mEGFP and Grl3p-pHluorin by western blotting using anti-GFP mAb **(Figure 3C)**. Importantly, by confocal microscopy we detected strong fluorescence signals for both Grl3p-mEGFP and Grl3p-pHluorin in docked mucocysts **(Figure 3D)**. Since the pHluorin signal in the easily identified docked mucocysts was not quenched, this result provides additional confirmation that mature mucocysts are not acidified. Since we could also detect non-quenched cytoplasmic pHluorin signal in non-cortical puncta, immature mucocysts may also be non-acidic.

To address the pH of mucocyst intermediates more rigorously, we endogenously tagged Grl3p in tandem with pHluorin followed by mCherry, whose fluorescence emission is not pH sensitive (Shaner et al., 2004, 2005; Doherty et al., 2010; Hundeshagen et al., 2011). By simultaneously collecting data in the red and green channels, we could detect acidic mucocysts (or mucocyst intermediates) as puncta showing red but not green fluorescence. In the docked mucocysts of wildtype cells (i.e., the cortical field), the large majority of red puncta also showed green fluorescence, with an overlap between signals of (Manders' Coefficients 0.78± SD 0.088) **(Figure 3E, top panel and 3F, right panel)**. In contrast, the overlap between green and red signals was significantly lower in non-cortical puncta (Manders' Coefficients 0.36± SD 0.13) **(Figure 3E, middle and bottom panels, and 3F, left panel)**. Thus, there is a significant population of Grl3p-containing, mucocyst-related puncta in the cytoplasm in which the pHluorin emission is quenched. This result strongly suggests that mucocysts are acidified at some stage in their formation.

A collection of mutant cell lines in *Tetrahymena* have characterized defects in mucocyst biogenesis or exocytosis. One such lines is MN173, in which the mucocysts undergo normal biochemical and morphological maturation but fail to dock at the plasma membrane and thus remain primarily dispersed in the cytoplasm (Chilcoat et al., 1996; Melia et al., 1998). We therefore expected that Grl3p-pHluorin-mCherry, expressed in MN173 cells, would produce non-cortical puncta with a strong overlap of green and red signals, from the non-acidic mature cytoplasmic mucocysts. Indeed, such cells showed complete co-localization of pHluorin and mCherry in the cytoplasm, supporting the validity of our approach **(Figure 3F, left panel and 3G)**. Taken together, our results strongly suggest that mucocysts are transiently acidified during their formation, while mature mucocysts are non-acidic.

The holo-V-ATPase complex does not persist during mucocyst maturation

Our localization data for V-ATPase a1, shown above, are consistent with the idea that this subunit is present in the transiently acidified immature non-cortical mucocysts, but also clearly

demonstrate that the subunit is still present in non-acidified mature docked mucocysts. We therefore asked whether other subunits of the V-ATPase complex were similarly localized, i.e., whether the V-ATPase is stably maintained during mucocyst maturation, or whether partial disassembly occurs so that some subunits are missing in mature mucocysts. To avoid the potential ambiguities that arise from studying genes that have paralogous copies, we focused on V-ATPase subunits encoded by single genes in *T. thermophila*. To begin, we used approaches including BLAST and structural homology to reveal that putative V_1 domain subunits in *Tetrahymena*, including Vma1p (subunit-A), Vma8p (subunit-D) and Vma10p (subunit-G) are expressed as single genes **(Table S1 and Figure S4A-E)**. The identity of these genes was determined using multiple approaches. The *T. thermophila* homologs for Vma1p, Vma8p and Vma10p) were found to have high sequence identity via BLAST with Vma subunits in the Opisthokont *S. cerevisiae* **(Table S1, Figure S4A-E)**. Consistent with the sequence identity, the Phyre2-predicted structures of Vma8p and Vma1p revealed high structural similarity with subunit-D and subunit-A of the V_1 domain of mammalian cells, respectively **(Figure S4A and S4B)**. *T. thermophila* Vma10p also showed predicted structural similarity to a V-ATPase subunit in *S. cerevisiae*, subunit-G, though this was more limited (62% coverage and 28% structural identity) **(Figure S4C)**. The predicted structural similarities between *T. thermophila* and human V-ATPase subunits were also supported by AlphaFold predictions, for subunit-D (**Figure S4D)** and subunit-A (**Figure S4E)** of *T. thermophila* (green) and human (blue). Taken together, these sequence and structural similarities strongly argue that these genes in *T. thermophila* encode components of the proton-translocating V-ATPase complex.

For each of these three V-ATPase subunits in *Tetrahymena*, each encoded by a single gene without paralogs, we then asked whether they were present in mucocysts. We imaged cells that endogenously co-expressed mCherry-tagged mucocyst marker Grl3p with mNeon-tagged Vma1p, Vma8p or Vma10p **(Figure 4A-J)**, and measured co-localization using the BIOP JACoP plugin in surface **(Figure 4A)** and cross sections **(Figure 4B)**. We found negligible overlap between the Vma subunits and Grl3p at the cell cortex in mature mucocysts **(Figure 4C, 4E, 4G and 4I)**. As expected, based on results shown above, there was instead complete overlap between Grl3p and V-ATPase-a1 at the cell cortex **(Figure 4K)**.

The non-cortical puncta showed striking differences from those at the cortex. In contrast to the results for mature mucocysts, we found significant overlap between Grl3p and all V-ATPase subunits (Vma1p, Vma8p, Vma10p and V-ATPase-a1p) at cytoplasmic puncta that reflect biosynthetic mucocyst intermediates **(Figure 4D, 4F, 4H, 4J and 4L)**.

Taken together, these results argue that multiple V-ATPase subunits, known to form part of the enzymatically-active holo-V-ATPase complex, are present in immature mucocysts. However, only a subset of those subunits persist in mature mucocysts docked at the cell surface. These results suggest that disassembly of the V-ATPase complex occurs during mucocyst maturation. The incompleteness of the V-ATPase complex present in mature mucocysts provides an explanation for why these organelles do not maintain an acidic lumenal environment.

***AP-3* is required for the de-acidification during mucocyst maturation**

The data outlined above reveal that disassembly of the V-ATPase holo-complex occurs during the maturation process and does not depend on docking *per se* since it occurs in the MN173 mutant. To begin identifying requirements for disassembly, we examined genes known to be required for mucocyst maturation. *Tetrahymena* lacking the μ-subunit of the AP-3 trafficking adaptor do not synthesize mature mucocysts but instead accumulate large spherical cytoplasmic vesicles bearing the proGrls (Kaur et al., 2017). We expressed Grl3p-pHluorin-mCherry in Δ*apm3* and analysed co-localization using BIOP JACoP plugin **(Figure 5A-D)**. In Δ*apm3* cells, the mCherry-positive puncta predominantly lacked pHluorin signal, indicating that the lumen of these mucocyst intermediates is acidic **(Figure 5B-C, S4F and Movie S2)**. There were also

puncta that showed green but not red signals, but these were consistently relatively few in number (**Figure 5D)**. It is known from studies in other organisms that deletion of AP-3µ leads to the loss of the entire AP-3 complex (Mullins et al., 2000; Cowles et al., 1997; Stepp et al., 1997). Our data therefore indicates that AP-3 activity is required for the transition from acidified mucocyst intermediates to neutral pH mature mucocysts.

V-ATPase-a1 is required for secretion from mucocysts

To ask if *V-ATPase-a1* were required for mucocyst biogenesis, we subcloned the 5'UTR and 3'UTR of the *V-ATPase-a1* gene into a pNeo4 knockout vector and transformed it into *Tetrahymena* by biolistic transformation to target the *V-ATPase-a1* gene for disruption via homologous recombination with a drug-resistance cassette. (**Figure 6A)**. During ~3-4 weeks of selection, all ~45 copies of a gene in the polyploid macronucleus can be replaced with the cassette, resulting in a functional knockout if the gene is nonessential (Coyne et al., 2008). After generating the *V-ATPase-a1* knockout line, called Δ*v-atpase-a1*, we used reverse transcription PCR (RT-PCR) to detect the gene transcript. The *V-ATPase-a1* transcript was not found in the deletion line (**Figure 6B**), which grew at wildtype rates under standard laboratory conditions. Hence the gene can be considered nonessential.

Mucocysts are secretory organelles, so defects in biogenesis result in reduced cargo secretion. We therefore tested the exocytic response of the knockout cell line using an assay in which brief exposure of wild-type cells to the calcium ionophore dibucaine triggers simultaneous secretion from the several thousand mucocysts per cell (Satir, 1977; Cowan et al., 2005; Kumar et al., 2014).We found that *Δv-atpase-a1* cells were grossly deficient in mucocyst content release **(Figure 6C)**.

V-ATPase-a1 is essential for mucocyst formation

To test whether *V-ATPase-a1* was required for mucocyst formation *per se*, we used indirect immunofluorescence with two monoclonal antibodies (mAbs) that recognize, respectively, Grl3p (mAb 5E9) and Grt1p (mAb 4D11) (Cowan et al., 2005; Kumar et al., 2014). Imaging of wild-type cells using either antibody brightly illuminates the mucocysts primarily docked at the cell periphery, as seen in cell cross sections **(Figure 6Di, iii and inset)**. In contrast, in *Δv-atpase-a1* cells both Grl3p and Grt1p were relatively sparse, and no mucocysts were docked at the cortex (**Figure 6Dii and iv)**. Notably, large fractions of the Grl3p and Grt1p in the *Δv-atpase-a1* cells are distant from the cell cortex (**Figure 6Dii and iv)**. *V-ATPase-a1* therefore is required for mucocyst formation. To further confirm it, we examined wild-type and *Δv-atpase-a1* cells **(Figure 6E, S5)** by electron microscopy. In wild-type cells, both immature mucocysts, as well as mature mucocysts docked at the cell cortex, were detected **(Figure 6E, i and ii)**. In the *Δv-atpase-a1* mutant, only structures resembling immature mucocysts were observed **(Figure 6E, iii and S5**).

V-ATPase-a1 is required for the processing of pro-Grl proteins

The dense lumenal proteinaceous core of mucocysts in wild-type cells is composed of GRL proteins, and the formation of the mucocyst core depends upon their proteolytic processing (Cowan et al., 2005; Turkewitz et al., 1991). The morphologically aberrant mucocysts in *Δv-atpase-a1* cells may be caused by defective processing of Grl proteins **(Figure 6D-E**). Therefore, we asked whether *V-ATPase-a1* were required for Grl proprotein processing. We analysed whole-cell lysates of the *Δv-atpase-a1* cells by Western blotting using anti-Grl antisera **(Figure 6F-G)**. In the mutant cells, the Grl proteins were found to accumulate as unprocessed or partially-processed precursors **(Figure 6F-G)**.

V-ATPase-a1 is required for a key membrane trafficking step during mucocyst formation

In addition to proteolytic maturation of Grl proproteins, a well-documented step in mucocyst formation is heterotypic vesicle fusion that brings together the Grl proteins, which may be trafficked directly from the Golgi/TGN, with Grt proteins as well as at least some key proGRL processing enzymes which may be trafficked via endosomes. This fusion step involves a Syntaxin 7-like homolog, Stx7l1 and the CORVET subunit Vps8a (Sparvoli et al., 2018). Stx7l1p itself, but not Vps8ap, remains associated with mature mucocysts. In cells lacking either *VPS8a* or *STX7l1*, Grl and Grt proteins accumulate in separate vesicles.

To test whether V-ATPase-a1 is required for heterotypic vesicle fusion, we used indirect immunofluorescence to localize Grt1p, Grl1p and Stx7l1p in fixed cells. In wildtype cells, Grl1p and Grt1p accumulate exclusively in docked mature mucocysts **(Figure 7A, top panel)**. In contrast, in *Δv-atpase-a1* cells, both cargo proteins accumulate in a heterogeneous cohort of cytoplasmic vesicles **(Figure 7A, middle panel)**. Compared to that in wild-type cells, Grl1p and Grt1p show significantly less overlap (~51%) in *Δv-atpase-a1* **(Figure 7B)**, which is similar to their overlap in *Δvps8a cells* **(Figure 7A, lower panel and 7B)**.

Consistent with previous results in wildtype cells (Kaur et al., 2017), Stx7l1p-GFP co-localized with Grt1p in docked mucocysts **(Figure 7C, top panel and S6A)**. Their co-localization is ~68% reduced in *Δv-atpase-a1* cells **(Figure 7C-D)**. Notably, a greater extent of co-localization is observed in the mutant cells between Grl3p and Stx7l1p **(Figure S6B-C)**. These results are consistent with earlier reports that Stx7l1p is associated with vesicles containing Grl3p rather than Grt1p (Kaur et al., 2017; Sparvoli et al., 2018). Our results suggest that the absence of V-ATPase-a1 inhibits heterotypic fusion between Grl- and Grt-containing vesicles.

We previously found evidence that the targeting of Grt1p to mucocysts depends on its interaction with a VPS10-family receptor, Sor4p (Briguglio et al., 2013). The Grt1p-containing vesicles in Δ*v-atpase-a1* cells, if they are stalled trafficking intermediates, might therefore also contain Sor4p. In agreement with this model, we found that the co-localization of Grt1p and Sor4p increased 3.5-fold in the Δ*v-atpase-a1* mutant compared to in wildtype cells **(Figure 7E-F, S6D)**. Taken together, our results support the idea that V-ATPase-a1p promotes fusion of Grl1p-containing and Sor4p/Grt1-containing vesicles during mucocyst formation, showing phenotypes similar to those seen in *Δvps8a* cells. Based on these data, we proposed a model for the mucocyst biogenesis pathway in *T. thermophila* **(Figure 8)**, extending the model proposed by Sparvoli *et al*, 2018.

Discussion

In *Tetrahymena thermophila*, the biogenesis of secretory vesicles known as mucocysts has previously been shown to depend on a set of proteins associated in other lineages with LROs (Kaur et al., 2017; Sparvoli et al., 2018). Here, we investigated whether a V-ATPase was also required for mucocyst formation. Based on genome annotation, *T. thermophila* expresses a large number of distinct V-ATPase subunits, many of which are likely to be compartment-specific. Among the 6 *T. thermophila* paralogs encoding a-subunits of the V_0 subcomplex, we discovered that the a1 paralog is transcriptionally coregulated with known mucocyst-associated genes, and that the corresponding protein localizes strongly, though not exclusively, to mature docked mucocysts. In other organisms, the localization specificity of V-ATPases has been shown to depend on determinants in the a-subunit of the V_0 subcomplex (Sun-Wada and Wada, 2013, 2022; Sun-Wada et al., 2007; Matsumoto et al., 2018; Oka et al., 2001; Chen et al., 2024; Capecci and Forgac, 2013; Toei et al., 2010). Consistent with this idea, in animal cells distinct a-subunits are found respectively in coated vesicles, the Golgi apparatus/early endosomes, and late endosomes/lysosomes (Breton and Brown, 2013; Chu et al., 2021; Matsumoto et al., 2018; Toei et al., 2010). The six genes encoding a-subunits of the V-ATPase in *T. thermophila* compare to just four a-subunit genes in mammals (Sun-Wada and Wada, 2013; Toei et al., 2010) while 17 a-subunit genes are present in *Paramecium tetraurelia* (Wassmer et al., 2006).

In *Paramecium*, these seventeen genes fell into nine families and localized to at least seven different compartments.

Notwithstanding the localization of a V-ATPase subunit to mucocysts, we demonstrate that they are similar to neutral pH storage LROs that have been documented in mammals, Amoebozoa, and other lineages. That is, we found by three different approaches that mature mucocysts, which dock at the plasma membrane, are not detectibly acidic. The most impactful of these approaches was based on tagging a mucocyst-cargo protein with pHluorin, a fluorophore whose emission is pH-sensitive, because it also allowed us to detect and analyze immature mucocysts. Using cells expressing this construct, we could detect mucocyst intermediates, i.e., cytoplasmic vesicles containing the mucocyst cargo protein Grl3p, that were acidified in contrast with mature mucocysts. Thus, our data strongly suggest that mucocysts are transiently acidified during their biogenesis. We found that the a1 subunit gene is non-essential but required for mucocyst biogenesis. Similarly, the a3 subunit in *Paramecium* had been implicated in the formation of trichocysts, which are homologous to mucocysts (Wassmer et al., 2006). The transient acidification of ciliate secretory LROs at an intermediate phase in organellar maturation may be sufficient to explain the defects seen with knockout or silencing of the V-ATPase complex subunit genes. At the same time, it remains possible that specific subunits, in either the intact or partially disassembled complex, play roles distinct from proton pumping.

In *Tetrahymena* we detected numerous defects in mucocyst formation in a1-knockout cells, including failure to process Grl proproteins as well as likely defects in heterotypic vesicle fusion that is a normal feature of mucocyst biogenesis. The proprotein processing defects are similar to those we previously found in cells lacking the gene encoding the key processing enzyme in mucocysts, *CTH3* (Kumar et al., 2014). These similarity in defects can be readily explained if transient acidification of the immature mucocyst is required to activate Cth3p. Similarly, the apparent defects in vesicle fusion, which resemble those in cells lacking the Vps8a subunit of a mucocyst-specific CORVET complex, could be indirect consequences of a failure to acidify one or more intermediates. However, such defects could also reflect a more direct role of one or more V-ATPase complex subunits in this step. The possibility that V-ATPases participate in some membrane fusion reactions, via mechanisms unrelated to their proton-pumping activity, has been a contentious issue, but includes recent support for a direct fusogenic role (Sreelatha et al., 2015; Strasser et al., 2011; Coonrod et al., 2013; El Far and Seagar, 2011; Wang and Hiesinger, 2013). Interestingly, in mammalian cells there is evidence that the V-ATPase on secretory vesicles acts to acidify the lumen but also to regulate exocytosis machinery by acting as a pH sensor (Poëa-Guyon et al., 2013). The issue of potential subunit activities that are independent of proton pumping is also relevant for subunits like a1 that remain mucocyst-associated after the holo-complex has disassembled during maturation.

We found that a significant fraction of a1-positive cytoplasmic puncta are also positive for Rab7. Rab7 was previously shown to be present on vesicles containing the mucocyst-destined protein Grt1p (Sparvoli et al., 2018). Consistent with this, we found significant colocalization between V-ATPase-a1p and Grt1p in cytoplasmic puncta that are likely intermediates in mucocyst biogenesis. The association of V-ATPase with Rab7 has also been reported in other cell types (Matsumoto et al., 2022, 2018; Matsumoto and Nakanishi-Matsui, 2019; Nakanishi-Matsui et al., 2024). Studies in osteoclasts demonstrated that subunit a3 recruits Rab7 to secretory lysosomes, promoting their transport to the cell periphery where they deliver bone-resorbing enzymes together with the proton pump. The a3 subunit has also been shown to be involved in the transport of Mon1A-Ccz1, a guanine nucleotide exchange factor (GEF) for Rab7, to secretory lysosomes (Matsumoto et al., 2022). Thus, the non-enzymatic roles of V-ATPase subunits include determinants for organelle transport (Matsumoto et al., 2018, 2022).

The physiological regulation of V-ATPase in mammals involves its reversible assembly/disassembly, among other mechanisms. For example, in yeast and mammalian cells

such reversible assembly of the V_1 and V_0 domains regulates endolysosomal/lysosomal pH (Lafourcade et al., 2008; Sava et al., 2024). Our results suggest that a similar phenomenon underlies the properties of mucocysts in *Tetrahymena*, unfolding in the context of an organellar maturation pathway. We found that V_1 subunits Vma1p, Vma8p and Vma10p are not present in mature, docked mucocysts, whereas they instead are found in a pool of cytoplasmic Grl3-positive puncta that are likely to represent immature mucocysts. These results suggest that the mucocyst-associated V-ATPase complex partially disassembles during maturation, with only a subset of the subunits remaining mucocyst-associated, which is correspondingly non-acidic. Importantly, at least one of the dissociated subunits, Vma8, has previously been shown to be essential for coupling of proton transport and ATP hydrolysis in yeast (Graham et al., 1995; Xu and Forgac, 2000). Therefore, the remnant V-ATPase complex in mature mucocysts is likely to be disabled for proton translocation, which can explain why mucocysts do not maintain an acidic luminal environment. Because non-acidic storage LROs are not unique to ciliates, similar phenomena could be an important feature of LRO specialization in other lineages.

The heterotetrameric trafficking adapter AP-3 is considered a conserved factor in LRO formation, and more broadly has a role in mediating cargo transport from the late/trans-Golgi to late endosomal compartments (Leih et al., 2024; Ma et al., 2021). We previously found that the AP-3 adapter was required for mucocyst formation, and speculated that it delivered an essential maturation factor. While the work in our current manuscript does not advance our understanding of the direct interactors of AP-3 in this pathway, we can now add significantly to the model by showing that AP-3 activity is required to promote disassembly of V-ATPase during mucocyst maturation. On this basis, we propose that AP-3 be considered a regulator of V-ATPase activity.

Materials And Methods

Reagents, *Tetrahymena* Strains and culture conditions

Tetrahymena thermophila strains were grown overnight at 30°C with agitation in nutrient rich SPP medium (2% proteose peptone, 0.2% dextrose, 0.1% yeast extract, 0.003% ferric EDTA) supplemented with 250 µg/ml streptomycin sulfate, 250 µg/ml penicillin G, and 0.25 µg/ml amphotericin B fungizone, to medium density (2-3 × 10^5 cells/ml). Cu428 wild type strain was used as a control for all experiments and for biolistic transformation. 10mM Tris buffer (pH 7.4) was used for washing cells and as a starvation medium to reduce autofluorescence in food vacuoles. Cell culture densities were measured using a hemocytometer. *T. thermophila* strains used in this study are listed in **Table 1**. All reagents, chemicals, plasmids, and other information are listed in Key Resources Supplemental **Table S2**. The constructs p2xHA-3xmCherry-Rab7p-NCVB, pGrl3p-GFP-CHX, pSor4p-GFP-CHX, p-2xmNeon-6c-myc-Neo4, p3xmCherry-2xHA-Neo4 and *Δvps8a*-Neo4 were from (Sparvoli et al., 2018); pmEGFP-Neo4 and pNeo4 KO vector were from (Kumar et al., 2014); pStx7l1p-GFP-Blasticidin was from (Kaur et al., 2017). Plasmids pPOC1-mCherry-BSR and pPur4 were generously provided by Prof. Chad Pearson (University of Colorado, USA) and Dr. Kazufumi Mochizuki (University of Montpellier, France), respectively. Wild type strain Cu428 was from Dr Abdur Rahaman (NISER, India).

Table 1: *Tetrahymena* Strains used in this study

Strain name	Phenotype	Details of relevant genetic modification	Source
Cu428	Wild type	None	Dr Abdur Rahaman (NISER, India)

MN173	Exocytosis (exo-) mutant, the mucocysts fail to dock at the plasma membrane	Unknown	(Chilcoat et al., 1996; Melia et al., 1998)
Δapm3	*Δapm3;* no detectible *APM3* expression.	Replace *APM3* with Neo4 cassette	(Kaur et al., 2017)
Igr1p-3xmCherry-2xHA	Endogenous-level expression of 3xmCherry-2xHA-tagged Igr1p	C-terminal fusion of Igr1p and 3xmCherry-2xHA with Pur4 cassette, integrated at the macronuclear *IGR1* locus	(Kuppannan et al., 2022)
SKBN001	*Δv-atpase-a1;* no detectible *V-ATPase-a1* expression	Replaces nucleotides 1 to 3479 bp of macronuclear V-ATPase-a1 ORF with Neo4 cassette.	This study
SKBN002	Endogenous-level expression of 2xmNeon-6xc-myc-tagged V-ATPase-a1p	C-terminal fusion of V-ATPase-a1p and 2xmNeon-6xc-myc with Neo4 cassette, integrated at the macronuclear *V-ATPase-a1* locus	This study
SKBN003	Endogenous-level expression of 3xmCherry-2xHA-tagged Grl3p	C-terminal fusion of Grl3p and 3xmCherry-2xHA with Pur4 cassette, integrated at the macronuclear *GRL3* locus	This study
SKBN004	Endogenous-level expression of 2xmNeon-6xc-myc-tagged V-ATPase-a1p and 3xmCherry-2xHA-tagged Grl3p	C-terminal fusion of V-ATPase-a1p and 2xmNeon-6xc-myc with Neo4 cassette, integrated at the macronuclear *V-ATPase-a1* locus. Also, C-terminal fusion of Grl3p and 3xmCherry-2xHA with Pur4 cassette, integrated at the macronuclear *GRL3* locus	This study
SKBN005	Endogenous-level expression of 2xmNeon-6xc-myc-tagged V-ATPase-a1p. Inducible expression of 2xHA-3xmCherry-tagged Rab7p	C-terminal fusion of V-ATPase-a1p and 2xmNeon-6xc-myc with Neo4 cassette, integrated at the macronuclear *V-ATPase-a1* locus. Also, N-terminal fusion of Rab7p and 2xHA-3xmCherry, expressed under the control of the *MTT1* promoter, at the macronuclear *MTT1* locus.	This study
SKBN006	Endogenous-level expression of 2xmNeon-6xc-myc-tagged V-ATPase-a2p and 3xmCherry-2xHA-tagged Grl3p	C-terminal fusion of V-ATPase-a2p and 2xmNeon-6xc-myc with Neo4 cassette, integrated at the macronuclear *V-ATPase-a2* locus. Also, C-terminal fusion of Grl3p and 3xmCherry-2xHA with Pur4 cassette, integrated at the macronuclear *GRL3* locus	This study
SKBN007	Endogenous-level expression of GFP-tagged Grl3p	C-terminal fusion of Grl3p and GFP with Neo4 cassette, integrated at the macronuclear *GRL3* locus	This study
SKBN008	Endogenous-level expression of pHluorin-tagged Grl3p	C-terminal fusion of Grl3p and pHluorin with Neo4 cassette, integrated at the macronuclear *GRL3* locus	This study
SKBN009	Endogenous-level expression of GFP-tagged Sor4p.	C-terminal fusion of Sor4p and GFP with CHX cassette, integrated at the macronuclear *SOR4* locus.	This study
SKBN010	Endogenous-level expression of GFP-tagged Sor4p. *Δv-atpase-a1;* no detectible *V-ATPase-a1* expression.	C-terminal fusion of Sor4p and GFP with CHX cassette, integrated at the macronuclear *SOR4* locus. Replaces nucleotides 1 to 3479 bp of macronuclear V-ATPase-a1 ORF with Neo4 cassette.	This study

SKBN011	Endogenous-level expression of 2xmNeon-6xc-myc-tagged Vma1p and 3xmCherry-2xHA-tagged Grl3p	C-terminal fusion of Vma1p and 2xmNeon-6xc-myc with Neo4 cassette, integrated at the macronuclear *VMA1* locus. Also, C-terminal fusion of Grl3p and 3xmCherry-2xHA with Pur4 cassette, integrated at the macronuclear *GRL3* locus	This study
SKBN012	Endogenous-level expression of 2xmNeon-6xc-myc-tagged Vma8p and 3xmCherry-2xHA-tagged Grl3p	C-terminal fusion of Vma8p and 2xmNeon-6xc-myc with Neo4 cassette, integrated at the macronuclear *VMA8* locus. Also, C-terminal fusion of Grl3p and 3xmCherry-2xHA with Pur4 cassette, integrated at the macronuclear *GRL3* locus	This study
SKBN013	Endogenous-level expression of 2xmNeon-6xc-myc-tagged Vma10p and 3xmCherry-2xHA-tagged Grl3p	C-terminal fusion of Vma10p and 2xmNeon-6xc-myc with Neo4 cassette, integrated at the macronuclear *VMA10* locus. Also, C-terminal fusion of Grl3p and 3xmCherry-2xHA with Pur4 cassette, integrated at the macronuclear *GRL3* locus	This study
SKBN014	Endogenous-level expression of pHluorin-mCherry tagged Grl3p	C-terminal fusion of Grl3p and pHluorin-mCherry with Pur4 cassette, integrated at the macronuclear *GRL3* locus of Cu428 cells	This study
SKBN015	Endogenous-level expression of pHluorin-mCherry tagged Grl3p. *Δapm3;* no detectible *APM3* expression.	C-terminal fusion of Grl3p and pHluorin-mCherry with Pur4 cassette, integrated at the macronuclear *GRL3* locus of *Δapm3* cells	This study
SKBN016	Endogenous-level expression of pHluorin-mCherry tagged Grl3p.	C-terminal fusion of Grl3p and pHluorin-mCherry with Pur4 cassette, integrated at the macronuclear *GRL3* locus of MN173 cells	This study
SKBN017	Inducible expression of GFP-tagged Stx7l1p.	C-terminal fusion of Stx7l1p and GFP with BLAS cassette, integrated at the macronuclear *MTT1* locus.	This study
SKBN018	Inducible expression of GFP-tagged Stx7l1p. *Δv-atpase-a1;* no detectible *V-ATPase-a1* expression.	C-terminal fusion of Xtx7l1p and GFP with BLAS cassette, integrated at the macronuclear *MTT1* locus. Replaces nucleotides 1 to 3479 bp of macronuclear V-ATPase-a1 ORF with Neo4 cassette.	This study

Exocytosis assay

Exocytosis was stimulated by dibucaine as described previously (Kumar et al., 2014; Rahaman et al., 2009).

Verification of knockouts of genes by reverse transcriptase (RT)-PCR

RT-PCR was performed as described previously (Kumar et al., 2014). Briefly, total RNA was extracted by following the manufacturer's instructions using RNeasy mini spin column kits (Qiagen, USA). cDNA (200-500 base pairs of each gene) was synthesized and further amplified using the one step RT-PCR kit (Qiagen USA,) as per manufacturer's protocol using primers designated in **Supplemental Table S3**. To provide positive controls, RT-PCR using β-tubulin specific primers were performed in parallel.

Biolistic transformation

Biolistic transformations were carried out as described (Kumar et al., 2015, 2014) with some modifications. Briefly, cells were grown in SPP medium and incubated at 30°C with swirling to reach medium cell density. The next day, cells were washed twice with 10 mM Tris pH 7.4 and starved in the same buffer for 16 to 18 hours. 15 μg of total linearized plasmid DNA were conjugated with 0.6 μ gold particles (Bio-Rad, USA) as per the manufacturer's instructions. Four hours after bombardment, drugs were added to cultures that were swirling at 30°C to select positive transformants. Positive transformants were identified after 3–4 days and serially transferred 5 days/week in increasing concentrations of drug and decreasing concentrations of $CdCl_2$ (up to 6.5 mg/ml of paromomycin, 0.1 μg/ml $CdCl_2$; up to 200 μg/ml of puromycin and 0.5 μg/ml $CdCl_2$; up to 60 μg/ml of blasticidin and 0.5 μg/ml $CdCl_2$, 20 μg/ml of cycloheximide and 0.8 μg/ml $CdCl_2$) for 4-5 weeks before further testing. Each line was evaluated using at least three independent transformants.

Generation of *V-ATPase-a1* knockout strain

Upstream (~1 kb) and downstream (~1 kb) regions of the *V-ATPase-a1* (TTHERM_01332070) gene were amplified by PCR and subcloned into the SacI and XhoI sites of the pNeo4 vector, respectively, using the In-Fusion cloning kit (TaKaRa, Japan). *V-ATPase-a1* knockout construct was linearized using KpnI and SapI enzymes before biolistic transformation into Cu428 cells. The entire sequence of the *V-ATPase-a1* gene was deleted. The primers used to amplify target regions are listed in **Supplemental Table S3**.

Live-cell microscopy

Cultures for live microscopy were analyzed at mid-density unless otherwise indicated. To image cells expressing mNeon, mCherry, GFP or pHluorin-tagged fusion proteins, transformants were cultured overnight in SPP media and then transferred into 10 mM Tris pH 7.4 for 2-4 h to reduce autofluorescence in food vacuoles. Co-localization in live cells was determined by simultaneous imaging of mNeon or GFP-tagged fusion proteins with mCherry-tagged mucocyst markers. To simultaneously localize mNeon tagged V-ATPase-a1p with Lyso-Tracker Red (Invitrogen, USA), cells were incubated with 200 nM Lyso-Tracker Red for 5 min and images were captured as previously described (Kumar et al., 2014). For co-localization of V-ATPase-a1p and FM4-64 (Invitrogen, USA), cells were treated with 5 μM FM4-64, which labels endosomes, for 5 minutes and then pelleted and resuspended in 10 mM Tris pH 7.4. Subsequently, cells were imaged within 30-40 minutes. Cells expressing Igr1p-3xmCherry were incubated with 0.1 μg/ml Acridine Orange (Invitrogen, USA) for 2 min, while cells expressing Grl3p-3xmCherry were incubated with 5 μM Protonex Green (AAT Bioquest, USA) for 120 min, both at room temperature and in the dark. Cells were washed twice with 10 mM Tris pH 7.4 and observed under the microscope. To check co-localization between V-ATPase-a1p and Rab7 positive endosomes, cells were transformed to co-express V-ATPAse-a1p at the endogenous locus with mCherry-Rab7p. Transgene mCherry-Rab7p was induced for 2h in SPP with 2 μg/ml $CdCl_2$ followed by induction with 0.5μg/ml $CdCl_2$ for 2h in starvation buffer 10 mM Tris, pH 7.4. Stx7l1p-GFP was induced with $CdCl_2$ as mentioned above. Live-cell images were captured using an Olympus SR10 spinning disk super-resolution confocal microscope (Olympus, Japan). Both confocal and super-resolution modes with a 60x oil objective were used to capture time-lapse videos. For z sectioning, SORA disk-enabled acquisition was used to keep the z slice step size at 0.3 μm. After removing the background signal from the images, they were saved as JPEGs that were denoised, colored, and adjusted for brightness and contrast using the Fiji application (http://fiji.sc/Fiji).

Immunofluorescence Assay

Cells were grown to reach a cell density of $5x10^5$ cells/ml, then starved in 10 mM Tris pH 7.4 for 2 hours, fixed, and immunolabeled as described previously (Kumar et al., 2014). Monoclonal antibodies 5E9 [1:9; (Bowman and Turkewitz, 2001)and 4D11 1:5; (Turkewitz and Kelly, 1992)] were used to visualize Grl3p and Grt1p, respectively followed by goat anti-mouse conjugated with Texas red (1:100; Invitrogen, USA). Grl1p and GFP-tagged fusion proteins were visualized by 1:5000 diluted rabbit anti-Grl1 (Kuppannan et al., 2022; Ota, 2018) , and rabbit anti-GFP (1:400; (Invitrogen, USA), respectively, followed by anti-rabbit antibody conjugated with Alexa 488 (1:250 Invitrogen, USA). Cells were double immunolabeled with mouse mAb 4D11 and rabbit anti-Grl1 to visualize the fusion of Grl1p and Grt1p-containing vesicles. Fixed cells were imaged on a Leica SP5 II STED-CW super-resolution laser scanning confocal microscope (Leica, Germany) or an Olympus SR10 spinning disk super-resolution confocal microscope. Images were analyzed as described above.

Electron microscopy

Cells were grown to reach high cell density (10^6/ml), washed with 10mM Tris media (pH 7.4), fixed, section stained and imaged as described previously (Kumar et al., 2015).

SDS-PAGE, and Western blotting

Whole cell lysates were prepared from $3x10^5$ cells as described (Kumar et al., 2014). Using mouse anti-c-Myc Agarose beads (Thermo Fisher Scientific, USA), 2xmNeon-6c-myc-tagged fusion proteins were immunoprecipitated from detergent lysates as previously described (Sparvoli et al., 2018). Samples were separated using SDS-PAGE and then transferred to 0.45µ PVDF membranes (Merck Millipore, USA) for western blots. Blots were blocked and probed with antibodies described previously (Turkewitz et al., 1991). The primary antibodies rabbit anti-Grl1, rabbit anti-Grl3 (Kumar et al., 2014, 2015), mouse monoclonal anti-GFP (Biolegend, USA) and anti-c-Myc (Sigma, USA) were diluted 1:2000, 1:800, 1:5000 and 1:4000, respectively. Proteins were visualized using Super Signal West Femto Maximum Sensitivity Substrate (Thermo Fisher Scientific, USA), and enhanced chemiluminescence horseradish peroxidase–linked anti-rabbit (Bio-Rad, USA), anti-mouse (Bio-Rad, USA),) and anti-mouse for IP (Abcam, UK), with the secondary antibodies diluted 1:5000, 1:5000, and 1:1000, respectively.

Expression of V-ATPase-a1p, V-ATPase-a2p, Vma1p, Vma8p, Vma10p, Cth3p, Grl3p and Igr1p at endogenous locus

The p2xmNeon-6c-myc-Neo4 and pmEGFP-Neo4 vectors were previously described (Sparvoli et al., 2018; Kumar et al., 2014; Briguglio et al., 2013). To create pV-ATPase-a1p-2xmNeon-6c-myc-Neo4, the genomic DNA of V-*ATPase*-a1 (TTHERM_01332070; 1462bp) without stop codon and 1000bp of V-*ATPase*-a1 downstream genomic region were amplified and cloned into p2xmNeon-6c-myc-Neo4 vector at NotI and XhoI sites, respectively, using In-Fusion Cloning (TaKaRa, Japan). The construct was named pV-ATPase-a1p-2xmNeon-6c-myc-Neo4 was linearised with KpnI and SacI, 2xmNeon-6c-myc was fused to the C-terminus of V-*ATPase*-a1 at the endogenous macronuclear locus via homologous recombination. The similar approach was used to amplify the genomic DNA without stop codon (~700-900bp) and downstream genomic sequence (~600-850bp) of other V-ATPase subunits *V-ATPase-a2* (TTHERM_00463420), *VMA1* (TTHERM_00339640), *VMA8* (TTHERM_00821870) and *VMA10* (TTHERM_00052460) for fusion of 2xmNeon-6c-myc to the C-terminus of V-ATPase subunits at the endogenous macronuclear locus. For the generation of pGrl3p-3xmCherry-2xHA-Pur4, the pGrl3p-GFP-CHX vector was used as template (Sparvoli et al., 2018). BamHI/SpeI sites were used to replace monomeric mGFP with p3xmCherry-2xHA, while PstI/HindIII sites were used to replace CHX (cycloheximide resistance gene) with Pur4 (puromycin resistance gene) to generate pGrl3p-3xmCherry-2xHA-Pur4 vector. The pmEGFP-

Neo4 and pGrl3p-3xmCherry-2xHA-Pur4 vectors were used to make the pGrl3p-mEGFP-Neo4 construct. The genomic (857 bp excluding stop codon) and downstream sequence (783bp) of *GRL3* gene were excised from pGrl3p-3xmCherry-Pur4 vector using BamHI/ SacI and HindIII/KpnI, respectively and ligated into pmEGFP-Neo4 vector at mentioned sites respectively using T4 DNA ligase (New England, Biolabs, USA). pGrl3p-mEGFP-Neo4 vector was used as template to generate pGrl3p-pHluorin-Neo4 construct. Super ecliptic pHluorin (SEP) variant sequence was derived from the pHluorin MT1-MMP vector (Lizárraga et al., 2009). The pHluorin gene (lacking stop codon), codon optimised for *Tetrahymena* using the IDT Codon optimization tool, was synthesized (Eurofins Genomics Pvt Ltd) with added BamHI/SpeI sites at 5' and 3' end of gene. Monomeric mGFP from pGrl3p-mEGFP-Neo4 was replaced with pHluorin using BamHI/SpeI sites to generate pGrl3p-pHluorin-Neo4. To construct pGrl3-pHluorin-mCherry-Pur4, the Neo4 cassette of pGrl3p-pHluorin-Neo4 was replaced by Pur4 from pGrl3-3xmCherry-Pur4 using Kpn1 and Pst1 sites to generate pGrl3-pHluorin-Pur4. mCherry gene fragment was amplified from pPOC1-mCherry-BSR using primers designated in **Supplemental Table S3** and cloned into pGrl3-pHluorin-Pur4 vector at the SpeI site using In-fusion cloning. All constructs were confirmed by DNA sequencing. The final constructs were linearized with SacI and KpnI before transformation. The p2xHA-3xmCherry-Rab7p-Ncvb construct was linearized by digestion with SfiI and transformed into cells expressing V-ATPase-a1p by biolistic transformation. pGrl3p-3xmCherry-2xHA-Pur4, pGrl3p-mEGFP-Neo4 and pGrl3p-pHluorin-Neo4 were transformed into wildtype Cu428 using biolistic transformation. pGrl3-pHluorin-mCherry-Pur4 vector was transformed into Cu428, *Δapm3* and MN173 cells. V-ATPase-a1p-2xmNeon-6c-myc-Neo4, pV-ATPase-a2p-2xmNeon-6c-myc-Neo4, pVma1p-2xmNeon-6c-myc-Neo4, pVma8p-2xmNeon-6c-myc-Neo4 and pVma10p-2xmNeon-6c-myc-Neo4 vectors were transformed into Cu428 cell expressing Grl3p-3xmCherry-2xHA-Pur4.

Phylogenetic tree construction

Protein BLAST (BLASTp) was used to identify homologs of V- ATPase-a1p (TTHERM_01332070; XP_001010002.1) in ciliates (*Paramecium*), apicomplexans (*Toxoplasma gondii), Arabidopsis thaliana, Caenorhabditis elegans, Drosophila melanogaster, Danio rerio,* and *Homo sapiens,* as shown in Supplemental **Table S4**. For tree construction, the top hits from each lineage were selected, assembled, and aligned using ClustalX (1.8). Phylogenetic trees were built using MEGA 11 software (Molecular Evolutionary Genetics Analysis: www.megasoftware.net/) with the maximum likelihood option, without gap regions and with1000 bootstrap replicates.

***In silico* analyses**

Protein sequences of V-ATPase-a subunit paralogs (a1p-a6p) were extracted from TGD (https://tet.ciliate.org/) and aligned using EMBOSS Needle (https://www.ebi.ac.uk/jdispatcher/psa/emboss_needle) using the default parameters. Transcription profiles were downloaded from the Tetrahymena Functional Genomics Database (http://tfgd.ihb.ac.cn) (Xiong et al., 2013, 2011; Miao et al., 2009). For plotting, each profile was normalized by setting the maximum expression level of the gene to 1. The V-ATPase-a1p structure was predicted using Protein Homology/Analogy Recognition Engine V 2.0 (Phyre 2), a web portal for protein modelling (Kelley et al., 2015). Structural homologs of the *T. thermophila* V-ATPase-a1p were identified using the AlphaFold Protein Structure Database (https://alphafold.ebi.ac.uk/).

Acknowledgements

We thank Dr Prasad Abnave (NCCS, Pune) for critical evaluation and valuable feedback on the manuscript and Dr Jomon Joseph for many helpful discussions. We heartily thank our lab members Shubham Yadav and Satya Santoshi for their continuous and generous support; Nikhat Khan for skilful technical assistance in all the above experiments. We are grateful to the confocal microscopy facility of NCCS for their valuable help with light microscopy. S.K.'s laboratory is funded by Department of Biotechnology (DBT), Ministry of Science and Technology India (BT/PR38584/MED/122/247/2020), Department of Science and Technology (DST), Ministry of Science and Technology India (CRG/2021/000732) and DBT/Wellcome Trust India Alliance (IA/I/22/2/506480). A.P.T. was supported by the National Science Foundation (MCB 1937326). We dedicate this work to our late Director Dr Mohan R. Wani.

Author contributions

Conceptualization, S.K., A.P. and A.P.T; Methodology, A.P., N. T. and D. S.; Data Analysis, S. K. and A. P.; Investigation and experiment S. K., A.P., N. T., D.S., V.M., and L.K.B.; Resources, S.K. A.P.T; Writing – Original Draft, S. K.; Writing – Review & Editing, S. K., A.P., D. S. and A.P.T; Visualization, A.P., and N. T.; Supervision, S.K.; Funding Acquisition, S.K.

Declaration of Interests

The authors declare no competing interests.

Data availability

Data will be made available on request.

References:

Banushi, B., and F. Simpson. 2022. Overlapping Machinery in Lysosome-Related Organelle Trafficking: A Lesson from Rare Multisystem Disorders. *Cells*. 11. doi:10.3390/cells11223702.

Benčina, M. 2013. Illumination of the Spatial Order of Intracellular pH by Genetically Encoded pH-Sensitive Sensors. *Sensors (Basel)*. 13:16736. doi:10.3390/S131216736.

Berruti, G., and C. Paiardi. 2011. Acrosome biogenesis: Revisiting old questions to yield new insights. *Spermatogenesis*. 1:95–98. doi:10.4161/spmg.1.2.16820.

Bodzęta, A., M. Kahms, and J. Klingauf. 2017. The Presynaptic v-ATPase Reversibly Disassembles and Thereby Modulates Exocytosis but Is Not Part of the Fusion Machinery. *Cell Rep*. 20:1348–1359. doi:10.1016/j.celrep.2017.07.040.

Bonifacino, J.S. 2004. Insights into the biogenesis of lysosome-related organelles from the study of the Hermansky-Pudlak syndrome. *Ann N Y Acad Sci*. 1038:103–114. doi:10.1196/ANNALS.1315.018.

Bowman, G.R., N.C. Elde, G. Morgan, M. Winey, and A.P. Turkewitz. 2005. Core formation and the acquisition of fusion competence are linked during secretory granule maturation in Tetrahymena. *Traffic*. 6:303–323. doi:10.1111/J.1600-0854.2005.00273.X.

BOWMAN, G.R., D.G.S. SMITH, K.W. MICHAEL SIU, R.E. PEARLMAN, and A.P. TURKEWITZ. 2005. Genomic and Proteomic Evidence for a Second Family of Dense Core Granule Cargo Proteins in *Tetrahymena thermophila*. *Journal of Eukaryotic Microbiology*. 52:291–297. doi:10.1111/j.1550-7408.2005.00045.x.

754 Bowman, G.R., and A.P. Turkewitz. 2001. Analysis of a mutant exhibiting conditional sorting to dense
755 core secretory granules in Tetrahymena thermophila. *Genetics*. 159:1605–1616.
756 doi:10.1093/GENETICS/159.4.1605.

757 Breton, S., and D. Brown. 2013. Regulation of Luminal Acidification by the V-ATPase. *Physiology*.
758 28:318–329. doi:10.1152/physiol.00007.2013.

759 Briguglio, J.S., S. Kumar, and A.P. Turkewitz. 2013. Lysosomal sorting receptors are essential for
760 secretory granule biogenesis in Tetrahymena. *J Cell Biol*. 203:537–550.
761 doi:10.1083/JCB.201305086.

762 Capecci, J., and M. Forgac. 2013. The function of vacuolar ATPase (V-ATPase) a subunit isoforms in
763 invasiveness of MCF10a and MCF10CA1a human breast cancer cells. *J Biol Chem*. 288:32731–
764 32741. doi:10.1074/jbc.M113.503771.

765 Chan, C.-Y., and K.J. Parra. 2014. Yeast phosphofructokinase-1 subunit Pfk2p is necessary for pH
766 homeostasis and glucose-dependent vacuolar ATPase reassembly. *J Biol Chem*. 289:19448–57.
767 doi:10.1074/jbc.M114.569855.

768 Chander, A., R.G. Johnson, J. Reicherter, and A.B. Fisher. 1986. Lung lamellar bodies maintain an
769 acidic internal pH. *J Biol Chem*. 261:6126–31.

770 Chen, Q., H. Kou, D. Lou Demy, W. Liu, J. Li, Z. Wen, P. Herbomel, Z. Huang, W. Zhang, and J. Xu.
771 2024. The different roles of V-ATPase a subunits in phagocytosis/endocytosis and autophagy.
772 *Autophagy*. doi:10.1080/15548627.2024.2366748.

773 Cheng, X.-T., Y.-X. Xie, B. Zhou, N. Huang, T. Farfel-Becker, and Z.-H. Sheng. 2018. Characterization of
774 LAMP1-labeled nondegradative lysosomal and endocytic compartments in neurons. *J Cell Biol*.
775 217:3127–3139. doi:10.1083/jcb.201711083.

776 Chilcoat, N.D., S.M. Melia, A. Haddad, and A.P. Turkewitz. 1996. Granule lattice protein 1 (Grl1p), an
777 acidic, calcium-binding protein in Tetrahymena thermophila dense-core secretory granules,
778 influences granule size, shape, content organization, and release but not protein sorting or
779 condensation. *J Cell Biol*. 135:1775–87. doi:10.1083/jcb.135.6.1775.

780 Chintagari, N.R., A. Mishra, L. Su, Y. Wang, S. Ayalew, S.D. Hartson, and L. Liu. 2010. Vacuolar ATPase
781 regulates surfactant secretion in rat alveolar type II cells by modulating lamellar body calcium.
782 *PLoS One*. 5:e9228. doi:10.1371/journal.pone.0009228.

783 Chu, A., R.A. Zirngibl, and M.F. Manolson. 2021. The V-ATPase a 3 Subunit: Structure, Function and
784 Therapeutic Potential of an Essential Biomolecule in Osteoclastic Bone Resorption. *Int J Mol Sci*.
785 22. doi:10.3390/IJMS22136934.

786 Coonrod, E.M., L.A. Graham, L.N. Carpp, T.M. Carr, L. Stirrat, K. Bowers, N.J. Bryant, and T.H. Stevens.
787 2013. Homotypic vacuole fusion in yeast requires organelle acidification and not the V-ATPase
788 membrane domain. *Dev Cell*. 27:462–8. doi:10.1016/j.devcel.2013.10.014.

789 Correia, M.S., H. Moreiras, F.J.C. Pereira, M. V Neto, T.C. Festas, A.K. Tarafder, J.S. Ramalho, M.C.
790 Seabra, and D.C. Barral. 2018. Melanin Transferred to Keratinocytes Resides in Nondegradative
791 Endocytic Compartments. *J Invest Dermatol*. 138:637–646. doi:10.1016/j.jid.2017.09.042.

792 Cowan, A.T., G.R. Bowman, K.F. Edwards, J.J. Emerson, and A.P. Turkewitz. 2005. Genetic, genomic,
793 and functional analysis of the granule lattice proteins in Tetrahymena secretory granules. *Mol
794 Biol Cell*. 16:4046–4060. doi:10.1091/MBC.E05-01-0028.

795 Cowles, C.R., G. Odorizzi, G.S. Payne, and S.D. Emr. 1997. The AP-3 adaptor complex is essential for
796 cargo-selective transport to the yeast vacuole. *Cell*. 91:109–18. doi:10.1016/s0092-
797 8674(01)80013-1.

798 Coyne, R.S., M. Thiagarajan, K.M. Jones, J.R. Wortman, L.J. Tallon, B.J. Haas, D.M. Cassidy-Hanley,
799 E.A. Wiley, J.J. Smith, K. Collins, S.R. Lee, M.T. Couvillion, Y. Liu, J. Garg, R.E. Pearlman, E.P.
800 Hamilton, E. Orias, J.A. Eisen, and B.A. Methé. 2008. Refined annotation and assembly of the
801 Tetrahymena thermophila genome sequence through EST analysis, comparative genomic
802 hybridization, and targeted gap closure. *BMC Genomics*. 9. doi:10.1186/1471-2164-9-562.

803 Delevoye, C., M.S. Marks, and G. Raposo. 2019. Lysosome-related organelles as functional
804 adaptations of the endolysosomal system. *Curr Opin Cell Biol*. 59:147–158.
805 doi:10.1016/j.ceb.2019.05.003.

806 Doherty, G.P., K. Bailey, and P.J. Lewis. 2010. Stage-specific fluorescence intensity of GFP and
807 mCherry during sporulation In Bacillus Subtilis. *BMC Res Notes*. 3:303. doi:10.1186/1756-0500-
808 3-303.

809 EC, D., M. C, C. S, and B. JS. 2000. Lysosome-related organelles. *FASEB J*. 14:1265–1278.
810 doi:10.1096/FJ.14.10.1265.

811 Eisen, J.A., R.S. Coyne, M. Wu, D. Wu, M. Thiagarajan, J.R. Wortman, J.H. Badger, Q. Ren, P. Amedeo,
812 K.M. Jones, L.J. Tallon, A.L. Delcher, S.L. Salzberg, J.C. Silva, B.J. Haas, W.H. Majoros, M. Farzad,
813 J.M. Carlton, R.K. Smith, J. Garg, R.E. Pearlman, K.M. Karrer, L. Sun, G. Manning, N.C. Elde, A.P.
814 Turkewitz, D.J. Asai, D.E. Wilkes, Y. Wang, H. Cai, K. Collins, B.A. Stewart, S.R. Lee, K.
815 Wilamowska, Z. Weinberg, W.L. Ruzzo, D. Wloga, J. Gaertig, J. Frankel, C.C. Tsao, M.A.
816 Gorovsky, P.J. Keeling, R.F. Waller, N.J. Patron, J.M. Cherry, N.A. Stover, C.J. Krieger, C. Del
817 Toro, H.F. Ryder, S.C. Williamson, R.A. Barbeau, E.P. Hamilton, and E. Orias. 2006.
818 Macronuclear genome sequence of the ciliate Tetrahymena thermophila, a model eukaryote.
819 *PLoS Biol*. 4:1620–1642. doi:10.1371/JOURNAL.PBIO.0040286.

820 El Far, O., and M. Seagar. 2011. A role for V-ATPase subunits in synaptic vesicle fusion? *J Neurochem*.
821 117:603–12. doi:10.1111/j.1471-4159.2011.07234.x.

822 Fok, A.K., M. Clarke, L. Ma, and R.D. Allen. 1993. Vacuolar H(+)-ATPase of Dictyostelium discoideum.
823 A monoclonal antibody study. *J Cell Sci*. 106 (Pt 4):1103–13. doi:10.1242/jcs.106.4.1103.

824 Forgac, M. 2007. Vacuolar ATPases: rotary proton pumps in physiology and pathophysiology. *Nat*
825 *Rev Mol Cell Biol*. 8:917–929. doi:10.1038/NRM2272.

826 Futai, M., G.H. Sun-Wada, Y. Wada, N. Matsumoto, and M. Nakanishi-Matsui. 2019. Vacuolar-type
827 ATPase: A proton pump to lysosomal trafficking. *Proc Jpn Acad Ser B Phys Biol Sci*. 95:261–277.
828 doi:10.2183/PJAB.95.018.

829 Gautam, R., E.K. Novak, J. Tan, K. Wakamatsu, S. Ito, and R.T. Swank. 2006. Interaction of
830 Hermansky-Pudlak Syndrome Genes in the Regulation of Lysosome-Related Organelles. *Traffic*.
831 7:779–792. doi:10.1111/j.1600-0854.2006.00431.x.

832 Graham, L.A., K.J. Hill, and T.H. Stevens. 1995. VMA8 encodes a 32-kDa V1 subunit of the
833 Saccharomyces cerevisiae vacuolar H(+)-ATPase required for function and assembly of the
834 enzyme complex. *J Biol Chem*. 270:15037–44. doi:10.1074/jbc.270.25.15037.

835 Griffiths, G.M., and Y. Argon. 1995. Structure and biogenesis of lytic granules. *Curr Top Microbiol*
836 *Immunol*. 198:39–58. doi:10.1007/978-3-642-79414-8_3.

837 Hermey, G. 2009. The Vps10p-domain receptor family. *Cell Mol Life Sci*. 66:2677–2689.
838 doi:10.1007/S00018-009-0043-1.

839 Huizing, M., A. Helip-Wooley, W. Westbroek, M. Gunay-Aygun, and W.A. Gahl. 2008. Disorders of
840 lysosome-related organelle biogenesis: clinical and molecular genetics. *Annu Rev Genomics*
841 *Hum Genet*. 9:359–386. doi:10.1146/ANNUREV.GENOM.9.081307.164303.

842 Hundeshagen, P., A. Hamacher-Brady, R. Eils, and N.R. Brady. 2011. Concurrent detection of
843 autolysosome formation and lysosomal degradation by flow cytometry in a high-content screen
844 for inducers of autophagy. *BMC Biol*. 9:38. doi:10.1186/1741-7007-9-38.

845 Hurbain, I., M. Romao, P. Sextius, E. Bourreau, C. Marchal, F. Bernerd, C. Duval, and G. Raposo. 2018.
846 Melanosome Distribution in Keratinocytes in Different Skin Types: Melanosome Clusters Are
847 Not Degradative Organelles. *J Invest Dermatol*. 138:647–656. doi:10.1016/j.jid.2017.09.039.

848 Kaur, H., D. Sparvoli, H. Osakada, M. Iwamoto, T. Haraguchi, and A.P. Turkewitz. 2017. An endosomal
849 syntaxin and the AP-3 complex are required for formation and maturation of candidate
850 lysosome-related secretory organelles (mucocysts) in Tetrahymena thermophila. *Mol Biol Cell*.
851 28:1551–1564. doi:10.1091/MBC.E17-01-0018.

852 Kawasaki-Nishi, S., T. Nishi, and M. Forgac. 2001. Yeast V-ATPase complexes containing different
853 isoforms of the 100-kDa a-subunit differ in coupling efficiency and in vivo dissociation. *J Biol*
854 *Chem*. 276:17941–17948. doi:10.1074/JBC.M010790200.

855 Kelley, L.A., S. Mezulis, C.M. Yates, M.N. Wass, and M.J.E. Sternberg. 2015. The Phyre2 web portal
856 for protein modeling, prediction and analysis. *Nat Protoc*. 10:845–858.
857 doi:10.1038/NPROT.2015.053.

858 Khan, M.M., S. Lee, S. Couoh-Cardel, R.A. Oot, H. Kim, S. Wilkens, and S.-H. Roh. 2022. Oxidative
859 stress protein Oxr1 promotes V-ATPase holoenzyme disassembly in catalytic activity-
860 independent manner. *EMBO J*. 41:e109360. doi:10.15252/embj.2021109360.

861 Khawar, M.B., H. Gao, and W. Li. 2019. Mechanism of Acrosome Biogenesis in Mammals. *Front Cell*
862 *Dev Biol*. 7. doi:10.3389/fcell.2019.00195.

863 Kumar, S., J.S. Briguglio, and A.P. Turkewitz. 2014. An aspartyl cathepsin, CTH3, is essential for
864 proprotein processing during secretory granule maturation in Tetrahymena thermophila. *Mol*
865 *Biol Cell*. 25:2444–2460. doi:10.1091/MBC.E14-03-0833.

866 Kumar, S., J.S. Briguglio, and A.P. Turkewitz. 2015. Secretion of Polypeptide Crystals from
867 Tetrahymena thermophila Secretory Organelles (Mucocysts) Depends on Processing by a
868 Cysteine Cathepsin, Cth4p. *Eukaryot Cell*. 14:817–833. doi:10.1128/EC.00058-15.

869 Kuppannan, A., Y.Y. Jiang, W. Maier, C. Liu, C.F. Lang, C.Y. Cheng, M.C. Field, M. Zhao, M. Zoltner, and
870 A.P. Turkewitz. 2022. A novel membrane complex is required for docking and regulated
871 exocytosis of lysosome-related organelles in Tetrahymena thermophila. *PLoS Genet*. 18.
872 doi:10.1371/JOURNAL.PGEN.1010194.

873 Lafourcade, C., K. Sobo, S. Kieffer-Jaquinod, J. Garin, and F.G. van der Goot. 2008. Regulation of the
874 V-ATPase along the endocytic pathway occurs through reversible subunit association and
875 membrane localization. *PLoS One*. 3:e2758. doi:10.1371/journal.pone.0002758.

876 Le, L., J. Sirés-Campos, G. Raposo, C. Delevoye, and M.S. Marks. 2021. Melanosome Biogenesis in the
877 Pigmentation of Mammalian Skin. *Integr Comp Biol*. 61:1517–1545. doi:10.1093/icb/icab078.

878 Leih, M., R.L. Plemel, M. West, C.G. Angers, A.J. Merz, and G. Odorizzi. 2024. Disordered hinge
879 regions of the AP-3 adaptor complex promote vesicle budding from the late Golgi in yeast. *J*
880 *Cell Sci*. 137. doi:10.1242/jcs.262234.

881 Lizárraga, F., R. Poincloux, M. Romão, G. Montagnac, G. Le Dez, I. Bonne, G. Rigaill, G. Raposo, and P.
882 Chavrier. 2009. Diaphanous-related formins are required for invadopodia formation and
883 invasion of breast tumor cells. *Cancer Res*. 69:2792–2800. doi:10.1158/0008-5472.CAN-08-
884 3709.

885 de Loubresse, N.G., M. Gautier, and L. Sperling. 1994. Immature secretory granules are not acidic in
886 *Paramecium* : Implications for sorting to the regulated pathway. *Biol Cell*. 82:139–147.
887 doi:10.1016/S0248-4900(94)80016-2.

888 Lu, M., D. Ammar, H. Ives, F. Albrecht, and S.L. Gluck. 2007. Physical interaction between aldolase
889 and vacuolar H+-ATPase is essential for the assembly and activity of the proton pump. *J Biol*
890 *Chem*. 282:24495–503. doi:10.1074/jbc.M702598200.

891 Lumpert, C.J., R. Glas-Albrecht, E. Eisenmann, and H. Plattner. 1992. Secretory organelles of
892 Paramecium cells (trichocysts) are not remarkably acidic compartments. *J Histochem*
893 *Cytochem*. 40:153–160. doi:10.1177/40.1.1370309.

894 Luzio, J.P., Y. Hackmann, N.M.G. Dieckmann, and G.M. Griffiths. 2014. The biogenesis of lysosomes
895 and lysosome-related organelles. *Cold Spring Harb Perspect Biol*. 6.
896 doi:10.1101/CSHPERSPECT.A016840.

897 Ma, Z., M.N. Islam, T. Xu, and E. Song. 2021. AP-3 adaptor complex-mediated vesicle trafficking.
898 *Biophys Rep*. 7:91–100. doi:10.52601/bpr.2021.200051.

899 Manolson, M.F., D. Proteau, R.A. Preston, A. Stenbit, B.T. Roberts, M.A. Hoyt, D. Preuss, J.
900 Mulholland, D. Botstein, and E.W. Jones. 1992. The VPH1 gene encodes a 95-kDa integral
901 membrane polypeptide required for in vivo assembly and activity of the yeast vacuolar H(+)-
902 ATPase. *Journal of Biological Chemistry*. 267:14294–14303. doi:10.1016/S0021-9258(19)49711-
903 1.

904 Manolson, M.F., B. Wu, D. Proteau, B.E. Taillon, B.T. Roberts, M.A. Hoyt, and E.W. Jones. 1994. STV1
905 gene encodes functional homologue of 95-kDa yeast vacuolar H(+)-ATPase subunit Vph1p. *J*
906 *Biol Chem*. 269:14064–14074. doi:10.1016/s0021-9258(17)36755-8.

907 Marks, M.S., H.F.G. Heijnen, and G. Raposo. 2013. Lysosome-related organelles: unusual
908 compartments become mainstream. *Curr Opin Cell Biol*. 25:495–505.
909 doi:10.1016/J.CEB.2013.04.008.

910 Martinière, A., G. Desbrosses, H. Sentenac, and N. Paris. 2013. Development and properties of
911 genetically encoded pH sensors in plants. *Front Plant Sci*. 4. doi:10.3389/FPLS.2013.00523.

912 Matsumoto, N., and M. Nakanishi-Matsui. 2019. Proton pumping V-ATPase inhibitor bafilomycin A1
913 affects Rab7 lysosomal localization and abolishes anterograde trafficking of osteoclast
914 secretory lysosomes. *Biochem Biophys Res Commun*. 510:421–426.
915 doi:10.1016/j.bbrc.2019.01.118.

916 Matsumoto, N., M. Sekiya, G.-H. Sun-Wada, Y. Wada, and M. Nakanishi-Matsui. 2022. The lysosomal
917 V-ATPase a3 subunit is involved in localization of Mon1-Ccz1, the GEF for Rab7, to secretory
918 lysosomes in osteoclasts. *Sci Rep*. 12:8455. doi:10.1038/s41598-022-12397-w.

919 Matsumoto, N., M. Sekiya, K. Tohyama, E. Ishiyama-Matsuura, G.H. Sun-Wada, Y. Wada, M. Futai,
920 and M. Nakanishi-Matsui. 2018. Essential Role of the a3 Isoform of V-ATPase in Secretory
921 Lysosome Trafficking via Rab7 Recruitment. *Sci Rep*. 8. doi:10.1038/S41598-018-24918-7.

922 McCormack, J.J., M. Lopes da Silva, F. Ferraro, F. Patella, and D.F. Cutler. 2017. Weibel−Palade
923 bodies at a glance. *J Cell Sci*. 130:3611–3617. doi:10.1242/jcs.208033.

924 Melia, S.M., E.S. Cole, and A.P. Turkewitz. 1998. Mutational analysis of regulated exocytosis in
925 Tetrahymena. *J Cell Sci*. 111 (Pt 1):131–40. doi:10.1242/jcs.111.1.131.

926 Metcalf, D.J., T.D. Nightingale, H.L. Zenner, W.W. Lui-Roberts, and D.F. Cutler. 2008. Formation and
927 function of Weibel-Palade bodies. *J Cell Sci*. 121:19–27. doi:10.1242/JCS.03494.

928 Miao, W., J. Xiong, J. Bowen, W. Wang, Y. Liu, O. Braguinets, J. Grigull, R.E. Pearlman, E. Orias, and
929 M.A. Gorovsky. 2009. Microarray Analyses of Gene Expression during the Tetrahymena
930 thermophila Life Cycle. *PLoS One*. 4:e4429. doi:10.1371/journal.pone.0004429.

931 Michaluk, P., and D.A. Rusakov. 2022. Monitoring cell membrane recycling dynamics of proteins
932 using whole-cell fluorescence recovery after photobleaching of pH-sensitive genetic tags. *Nat*
933 *Protoc*. 17:3056–3079. doi:10.1038/S41596-022-00732-4.

934 More, K.J., J.G.G. Kaufman, J.B. Dacks, and P.T. Manna. 2024. Evolutionary origins of the lysosome-
935 related organelle sorting machinery reveal ancient homology in post-endosome trafficking
936 pathways. *Proc Natl Acad Sci U S A*. 121:e2403601121. doi:10.1073/pnas.2403601121.

937 Mullins, C., L.M. Hartnell, and J.S. Bonifacino. 2000. Distinct requirements for the AP-3 adaptor
938 complex in pigment granule and synaptic vesicle biogenesis in Drosophila melanogaster. *Mol*
939 *Gen Genet*. 263:1003–1014. doi:10.1007/PL00008688.

940 Nakanishi-Matsui, M., N. Matsumoto, G.H. Sun-Wada, and Y. Wada. 2024. Role of the Cytosolic
941 Domain of the a3 Subunit of V-ATPase in the Interaction with Rab7 and Secretory Lysosome
942 Trafficking in Osteoclasts. *Biol Pharm Bull*. 47:339–344. doi:10.1248/BPB.B23-00833.

943 Naß, J., J. Terglane, and V. Gerke. 2021. Weibel Palade Bodies: Unique Secretory Organelles of
944 Endothelial Cells that Control Blood Vessel Homeostasis. *Front Cell Dev Biol*. 9:813995.
945 doi:10.3389/fcell.2021.813995.

946 Oka, T., T. Toyomura, K. Honjo, Y. Wada, and M. Futai. 2001. Four subunit a isoforms of
947 Caenorhabditis elegans vacuolar H+-ATPase. Cell-specific expression during development. *J Biol*
948 *Chem*. 276:33079–85. doi:10.1074/jbc.M101652200.

949 Oot, R.A., S. Couoh-Cardel, S. Sharma, N.J. Stam, and S. Wilkens. 2017. Breaking up and making up:
950 The secret life of the vacuolar H+ -ATPase. *Protein Sci*. 26:896–909. doi:10.1002/pro.3147.

951 Ota, T. 2018. Grl1 Protein is a Candidate K Antigen in Tetrahymena thermophila. *Protist*. 169:321–
952 332. doi:10.1016/J.PROTIS.2018.03.004.

953 Padh, H., J. Ha, M. Lavasa, and T.L. Steck. 1993. A post-lysosomal compartment in Dictyostelium
954 discoideum. *J Biol Chem*. 268:6742–7.

955 Parra, K.J., C.-Y. Chan, and J. Chen. 2014. Saccharomyces cerevisiae vacuolar H+-ATPase regulation
956 by disassembly and reassembly: one structure and multiple signals. *Eukaryot Cell*. 13:706–14.
957 doi:10.1128/EC.00050-14.

958 Parra, K.J., and P.M. Kane. 1998. Reversible association between the V1 and V0 domains of yeast
959 vacuolar H+-ATPase is an unconventional glucose-induced effect. *Mol Cell Biol*. 18:7064–74.
960 doi:10.1128/MCB.18.12.7064.

961 Pejler, G., J.M. Hu Frisk, D. Sjöström, A. Paivandy, and H. Öhrvik. 2017. Acidic pH is essential for
962 maintaining mast cell secretory granule homeostasis. *Cell Death Dis*. 8:e2785.
963 doi:10.1038/cddis.2017.206.

964 Plattner, H. 2017. Trichocysts-Paramecium's Projectile-like Secretory Organelles: Reappraisal of their
965 Biogenesis, Composition, Intracellular Transport, and Possible Functions. *J Eukaryot Microbiol*.
966 64:106–133. doi:10.1111/jeu.12332.

967 Poëa-Guyon, S., M.R. Ammar, M. Erard, M. Amar, A.W. Moreau, P. Fossier, V. Gleize, N. Vitale, and
968 N. Morel. 2013. The V-ATPase membrane domain is a sensor of granular pH that controls the
969 exocytotic machinery. *J Cell Biol*. 203:283–298. doi:10.1083/JCB.201303104.

970 Prakash, P., K.P. Jethava, N. Korte, P. Izquierdo, E. Favuzzi, I.V.L. Rose, K.A. Guttenplan, P.
971 Manchanda, S. Dutta, J.C. Rochet, G. Fishell, S.A. Liddelow, D. Attwell, and G. Chopra. 2021.
972 Monitoring phagocytic uptake of amyloid β into glial cell lysosomes in real time. *Chem Sci*.
973 12:10901–10918. doi:10.1039/D1SC03486C.

974 Rahaman, A., W. Miao, and A.P. Turkewitz. 2009. Independent transport and sorting of functionally
975 distinct protein families in Tetrahymena thermophila dense core secretory granules. *Eukaryot*
976 *Cell*. 8:1575–1583. doi:10.1128/EC.00151-09.

977 Raposo, G., M.S. Marks, and D.F. Cutler. 2007. Lysosome-related organelles: driving post-Golgi
978 compartments into specialisation. *Curr Opin Cell Biol*. 19:394–401.
979 doi:10.1016/J.CEB.2007.05.001.

980 Satir, B. 1977. Dibucaine-induced synchronous mucocyst secretion in Tetrahymena. *Cell Biol Int Rep*.
981 1:69–73. doi:10.1016/0309-1651(77)90012-1.

982 Sautin, Y.Y., M. Lu, A. Gaugler, L. Zhang, and S.L. Gluck. 2005. Phosphatidylinositol 3-kinase-mediated
983 effects of glucose on vacuolar H+-ATPase assembly, translocation, and acidification of
984 intracellular compartments in renal epithelial cells. *Mol Cell Biol*. 25:575–89.
985 doi:10.1128/MCB.25.2.575-589.2005.

986 Sava, I., L.J. Davis, S.R. Gray, N.A. Bright, and J.P. Luzio. 2024. Reversible assembly and disassembly of
987 V-ATPase during the lysosome regeneration cycle. *Mol Biol Cell*. 35:ar63. doi:10.1091/mbc.E23-
988 08-0322.

989 Shaner, N.C., R.E. Campbell, P.A. Steinbach, B.N.G. Giepmans, A.E. Palmer, and R.Y. Tsien. 2004.
990 Improved monomeric red, orange and yellow fluorescent proteins derived from Discosoma sp.
991 red fluorescent protein. *Nat Biotechnol*. 22:1567–72. doi:10.1038/nbt1037.

992 Shaner, N.C., P.A. Steinbach, and R.Y. Tsien. 2005. A guide to choosing fluorescent proteins. *Nat*
993 *Methods*. 2:905–9. doi:10.1038/nmeth819.

994 Smardon, A.M., N.D. Nasab, M. Tarsio, T.T. Diakov, and P.M. Kane. 2015. Molecular Interactions and
995 Cellular Itinerary of the Yeast RAVE (Regulator of the H+-ATPase of Vacuolar and Endosomal
996 Membranes) Complex. *J Biol Chem*. 290:27511–23. doi:10.1074/jbc.M115.667634.

997 Sparvoli, D., E. Richardson, H. Osakada, X. Lan, M. Iwamoto, G.R. Bowman, C. Kontur, W.A. Bourland,
998 D.H. Lynn, J.K. Pritchard, T. Haraguchi, J.B. Dacks, and A.P. Turkewitz. 2018. Remodeling the

999 Specificity of an Endosomal CORVET Tether Underlies Formation of Regulated Secretory
1000 Vesicles in the Ciliate Tetrahymena thermophila. *Curr Biol*. 28:697-710.e13.
1001 doi:10.1016/J.CUB.2018.01.047.

1002 Sreelatha, A., T.L. Bennett, E.M. Carpinone, K.M. O'Brien, K.D. Jordan, D.L. Burdette, K. Orth, and V.J.
1003 Starai. 2015. Vibrio effector protein VopQ inhibits fusion of V-ATPase-containing membranes.
1004 *Proc Natl Acad Sci U S A*. 112:100–105. doi:10.1073/PNAS.1413764111.

1005 Starcevic, M., R. Nazarian, and E.C. Dell'Angelica. 2002. The molecular machinery for the biogenesis
1006 of lysosome-related organelles: lessons from Hermansky-Pudlak syndrome. *Semin Cell Dev Biol*.
1007 13:271–278. doi:10.1016/S1084952102000563.

1008 Stepp, J.D., K. Huang, and S.K. Lemmon. 1997. The yeast adaptor protein complex, AP-3, is essential
1009 for the efficient delivery of alkaline phosphatase by the alternate pathway to the vacuole. *J Cell*
1010 *Biol*. 139:1761–74. doi:10.1083/jcb.139.7.1761.

1011 Stransky, L.A., and M. Forgac. 2015. Amino Acid Availability Modulates Vacuolar H+-ATPase
1012 Assembly. *J Biol Chem*. 290:27360–27369. doi:10.1074/jbc.M115.659128.

1013 Strasser, B., J. Iwaszkiewicz, O. Michielin, and A. Mayer. 2011. The V-ATPase proteolipid cylinder
1014 promotes the lipid-mixing stage of SNARE-dependent fusion of yeast vacuoles. *EMBO J*.
1015 30:4126–41. doi:10.1038/emboj.2011.335.

1016 Sun-Wada, G.H., H. Tabata, N. Kawamura, M. Futai, and Y. Wada. 2007. Differential expression of a
1017 subunit isoforms of the vacuolar-type proton pump ATPase in mouse endocrine tissues. *Cell*
1018 *Tissue Res*. 329:239–248. doi:10.1007/S00441-007-0421-7.

1019 Sun-Wada, G.-H., T. Toyomura, Y. Murata, A. Yamamoto, M. Futai, and Y. Wada. 2006. The *a* 3
1020 isoform of V-ATPase regulates insulin secretion from pancreatic β-cells. *J Cell Sci*. 119:4531–
1021 4540. doi:10.1242/jcs.03234.

1022 Sun-Wada, G.-H., and Y. Wada. 2013. Vacuolar-type proton pump ATPases: acidification and
1023 pathological relationships. *Histol Histopathol*. 28:805–15. doi:10.14670/HH-28.805.

1024 Sun-Wada, G.-H., and Y. Wada. 2022. The a subunit isoforms of vacuolar-type proton ATPase exhibit
1025 differential distribution in mouse perigastrulation embryos. *Sci Rep*. 12:13590.
1026 doi:10.1038/s41598-022-18002-4.

1027 Sun-Wada, G.-H., Y. Wada, and M. Futai. 2003. Lysosome and lysosome-related organelles
1028 responsible for specialized functions in higher organisms, with special emphasis on vacuolar-
1029 type proton ATPase. *Cell Struct Funct*. 28:455–63. doi:10.1247/csf.28.455.

1030 Toei, M., R. Saum, and M. Forgac. 2010. Regulation and isoform function of the V-ATPases.
1031 *Biochemistry*. 49:4715–23. doi:10.1021/bi100397s.

1032 Trombetta, E.S., M. Ebersold, W. Garrett, M. Pypaert, and I. Mellman. 2003. Activation of lysosomal
1033 function during dendritic cell maturation. *Science*. 299:1400–3. doi:10.1126/science.1080106.

1034 Turkewitz, A.P. 2004. Out with a bang! Tetrahymena as a model system to study secretory granule
1035 biogenesis. *Traffic*. 5:63–68. doi:10.1046/J.1600-0854.2003.00155.X.

1036 Turkewitz, A.P., and R.B. Kelly. 1992. Immunocytochemical analysis of secretion mutants of
1037 Tetrahymena using a mucocyst-specific monoclonal antibody. *Dev Genet*. 13:151–159.
1038 doi:10.1002/DVG.1020130209.

Turkewitz, A.P., L. Madeddu, and R.B. Kelly. 1991. Maturation of dense core granules in wild type and mutant Tetrahymena thermophila. *EMBO J*. 10:1979–1987. doi:10.1002/J.1460-2075.1991.TB07727.X.

Wang, D., and P.R. Hiesinger. 2013. The vesicular ATPase: a missing link between acidification and exocytosis. *J Cell Biol*. 203:171–3. doi:10.1083/jcb.201309130.

Wasmeier, C., M. Romao, L. Plowright, D.C. Bennett, G. Raposo, and M.C. Seabra. 2006. Rab38 and Rab32 control post-Golgi trafficking of melanogenic enzymes. *J Cell Biol*. 175:271–281. doi:10.1083/JCB.200606050.

Wassmer, T., R. Kissmehl, J. Cohen, and H. Plattner. 2006. Seventeen a-subunit isoforms of paramecium V-ATPase provide high specialization in localization and function. *Mol Biol Cell*. 17:917–30. doi:10.1091/mbc.e05-06-0511.

Weaver, T.E., C.-L. Na, and M. Stahlman. 2002. Biogenesis of lamellar bodies, lysosome-related organelles involved in storage and secretion of pulmonary surfactant. *Semin Cell Dev Biol*. 13:263–70. doi:10.1016/s1084952102000551.

Xiong, J., X.Y. Lu, Y.M. Lu, H.H. Zeng, D.X. Yuan, L.F. Feng, Y. Chang, J. Bowen, M. Gorovsky, C.J. Fu, and W. Miao. 2011. Tetrahymena Gene Expression Database (TGED): a resource of microarray data and co-expression analyses for Tetrahymena. *Sci China Life Sci*. 54:65–67. doi:10.1007/S11427-010-4114-1.

Xiong, J., Y. Lu, J. Feng, D. Yuan, M. Tian, Y. Chang, C. Fu, G. Wang, H. Zeng, and W. Miao. 2013. Tetrahymena functional genomics database (TetraFGD): an integrated resource for Tetrahymena functional genomics. *Database (Oxford)*. 2013. doi:10.1093/DATABASE/BAT008.

Xu, T., and M. Forgac. 2000. Subunit D (Vma8p) of the yeast vacuolar H+-ATPase plays a role in coupling of proton transport and ATP hydrolysis. *J Biol Chem*. 275:22075–81. doi:10.1074/jbc.M002983200.

Xu, T., and M. Forgac. 2001. Microtubules are involved in glucose-dependent dissociation of the yeast vacuolar [H+]-ATPase in vivo. *J Biol Chem*. 276:24855–61. doi:10.1074/jbc.M100637200.

Yap, C.C., L. Digilio, L.P. McMahon, A.D.R. Garcia, and B. Winckler. 2018. Degradation of dendritic cargos requires Rab7-dependent transport to somatic lysosomes. *J Cell Biol*. 217:3141–3159. doi:10.1083/jcb.201711039.

Figure Legends

Figure 1. (A) Expression profiling identifies a subunit of the V-ATPase complex (V-ATPase-a1) that is highly coregulated with known mucocyst associated genes (*GRL1*, *GRT1* and *CTH3*). Transcript data were retrieved from the Tetrahymena Functional Genomics Database (TFGD). For plotting the profiles, each value was normalized to the respective gene's maximum expression level. (B) Other paralogs of the *V-ATPase-a* subunit (*a2-a6*) are not coregulated with known mucocyst genes. (C) The predicted structure of V-ATPase-a1p of *Tetrahymena* by the web portal Phyre2. The image colors are ordered like the rainbow, from the N to the C terminus. (D-E) The predicted structure of V-ATPase-a1p of *Tetrahymena thermophila* (green), *Saccharomyces cerevisiae* (yellow) and *Mus musculus* (red) by AlphaFold structure

prediction. V-ATPase-a1p structure of *Tetrahymena thermophila* superimposed with V-ATPase-a1p of *Saccharomyces cerevisiae* (D) and *Mus musculus* (E) by PyMOL software.

Figure 2. Expression and localization of V-ATPase-a1p. (A) Detergent solutes of cells expressing V-ATPase-a1p were immunoprecipitated using anti-c-Myc Agarose beads. Pull down samples were separated by SDS-PAGE and blotted with mouse monoclonal anti-c-myc antibody. Blots were incubated with anti-mouse-IgG-HRP for IP and developed by SuperSignal West Femto Maximum Sensitivity Substrate. The expected size-specific band was only found in the V-ATPase-a1p lane. (B) In optical surface and cross section (left and right, respectively), images of cells endogenously expressing 2xmNeon-6c-myc-tagged V-ATPase-a1p subunit were acquired by super resolution confocal microscopy with low exposure conditions. At the cell surface, linear arrays of fluorescent puncta correspond to docked mucocysts, which show up in cross sections of the same cells as elongated vesicles. The inset reveals that V-ATPase-a1p accumulates in these docked mature mucocysts. (C) Cartoon representing localization of V-ATPase-a1p at cortical and non-cortical compartments of cells. (D) The mean fluorescence intensity associated with cell (B1), cortical (B2), and non- cortical (B3) was measured and converted to integrated density. Most V-ATPase-a1p is found in non-cortical compartments. (E) Cells co-expressing V-ATPase-a1p-2xmNeon with mucocyst marker Grl3p-3xmCherry, both at endogenous loci. V-ATPase-a1p and Grl3p overlap extensively at docked mucocysts. Images are shown as single slices, for clarity. The inset Ei depicts co-localization of V-ATPase-a1p with Grl3p. To measure co-localization, the images were processed to remove noise and adjust the thresholds, with co-localization quantified using the Fiji-BIOP JACoP plugin. (F) 20 non-overlapping images from panels E were used to calculate the percentage of overlap (Mander's coefficient) between V-ATPase-a1p and Grl3p in cortical (surface section) and non-cortical (cross section) domains. The error bars show the SDs. (G) V-ATPase-a1p in non-cortical puncta shows some overlap with endosomal marker FM4-64. Cells expressing V-ATPase-a1p-2xmNeon were incubated for 5 min with 5μM FM4-64 and then washed with 10mM Tris media (pH 7.4). Images were acquired after 30-40 minutes. (H) The inset (H) is from panel 2G. (I) 10 non-overlapping images from panels 2G were used to calculate the percentage of overlap (Mander's coefficient) between V-ATPase-a1p-2xmNeon and FM4-64 in non-cortical puncta. Scale bars, 10 μm.

Figure 3. The mucocyst lumen is not stably acidic. (A) Cells expressing mucocyst cargo Igr1p-3xmCherry incubated with Acridine Orange (AO). There is minimal overlap between AO and Igr1p in docked mucocysts. Confocal images are shown as single slices, corresponding to cross or surface sections, for clarity. (B) Protonex Green incubated with cells expressing mucocyst cargo Grl3p-3xmCherry. No significant co-localization is seen between Protonex Green and Grl3p in docked mucocysts. (C) Cell lysates (60,000 cell equivalents) were separated using SDS-PAGE, transferred to PVDF and probed with anti-GFP mAb, which also recognizes pHluorin. Bands corresponding to Grl3p-GFP and Grl3p-pHluorin are indicated by an asterisk. (D) Grl3p-GFP and Grl3p-pHluorin constructs were expressed at the native *GRL3* locus. The Super ecliptic pHluorin (SEP) only emits fluorescence at pH 6.5 or higher. Both Grl3p-GFP and Grl3p-pHluorin show strong signals in docked mucocysts, consistent with their characterization as a non-acidic compartment. (E-G) Endogenous expression of Grl3p-pHluorin-mCherry in Cu428 (wild type) and mutant MN173 cells. (E) In wild type cells, dual emission from both pHluorin and mCherry at each fluorescent spot was measured as co-localization, and was analyzed in cell surface (top) and cross-sections (middle). The images were processed to remove noise and adjust thresholds, with co-localization quantified using the Fiji-BIOP JACoP plugin. The edges of the cross-sections were excluded (marked by a green boundary line in the illustration on the left) to restrict analysis to non-cortical structures. To minimize false co-localization due to the bright autofluorescence from large food vacuoles, we

selected areas lacking food vacuoles (bottom) for quantitative analysis. The color images at the bottom illustrate co-localization in selected non-cortical regions, while the grey images reveal co-localization after threshold adjustments for the green and red channels. Surface sections were analyzed to measure co-localization in cortical structures. The pHluorin and mCherry signals showed complete overlap within the docked mucocysts. There was also significant co-localization of red and green signals in non-cortical structures, as shown in cross-sections of the same cells. (F) 12 non-overlapping images from panels E and G were analysed for both non-cortical (left) and cortical puncta (right). (G) Co-localization was measured in cross-sections of MN173 cells, as shown in panel E. Significant overlap of green and red signals was observed in the non-cortical region. The error bars show the SDs. Scale bars, 10 μm.

Figure 4. The V-ATPase complex in mature, but not immature, mucocysts lacks multiple subunits. (A-B) The co-localization of Vma subunits and Grl3p was measured using cell surface (A) and cross (B) sections. For the former, the edge of the cross-sections was excluded (indicated by green boundary line in cartoon, panel B) in order to measure colocalization in non-cortical structures. The surface sections (panel A) were used to measure colocalization in cortical structures. To reduce false co-localization in cortical sections due to the bright signal from the contractile vacuole near the cell posterior, only the anterior ~half of the cell was analyzed. (C-H) Cells co-expressing 2xmNeon-tagged Vma1p (C-D), Vma8p (E-F), and Vma10p (G-H) with the mucocyst marker Grl3p-3xmCherry, all at their endogenous loci. In both cross and surface sections, Vma subunits are localized at the contractile vacuoles (CVs) and in non-cortical puncta, as well as at the cell cortex. Co-localization was measured using the Fiji-BIOP JACoP plugin, as shown in panel A and B. The color images at the bottom show co-localization in selected non-cortical (cross section) and cortical compartments (surface section). Grey images show co-localization after adjusting the thresholds for the green and red channels. There was no co-localization of Vma subunits with Grl3p in mature, docked mucocysts at the cell cortex. In contrast, there was significant overlap between Grl3p and the Vma subunits in non-cortical compartments. (I-J). 20 non-overlapping images from panels C-H, K and L were used to calculate the percentage of overlap (Mander's coefficient) between Grl3p and V-ATPase subunits (Vma1p, Vma8p, Vma10p and V-ATPase-a1p) in cortical (I) and non-cortical compartments (J). The error bars show the SDs. (K-L) Co-expression of V-ATPase-a1p-2xmNeon and Grl3p-3xmCherry. In the surface section, there was complete overlap between Grl3p and V-ATPase-a1p, in the docked mucocysts. There was also significant co-localization of V-ATPase-a1p and Grl3p in non-cortical structures, as seen in cross-sections of the same cells. Scale bars, 10 μm.

Figure 5. The disassembly of the V-ATPase holo-complex requires AP-3. (A) Cartoon depicting the maturation of mucocysts in *Tetrahymena*. (B) The co-localization of green and red signals from Grl3p-pHluorin-mCherry expressed in Δ*apm3* cells, as shown in Figure 3E. In *Δapm3* cells, some co-localization of Grl3p was observed in the green and red channels within non-cortex compartments (C) Twelve separate images from panel B were analysed for non-cortical compartment. (D) Fluorescent puncta were quantified in both green and red channels from twelve separate images in panel B. The images were processed to remove noise, adjust thresholds and count fluorescent puncta using the Analyze Particles application in Image Fiji. Only particles ranging from 0.1 to 5 microns in size were counted to exclude background noise and large food vacuoles. The error bars show the SDs. Scale bars, 10 μm.

Figure 6. Analysis of the role of *V-ATPase-a1* in mucocyst biogenesis. (A) *V-ATPase-a1* knockout by homologous recombination. The knockout construct is described in Materials and Methods. (B) Confirmation of *V-ATPase-a1* knockout by one-step RT-PCR. PCR primers are listed in Supplemental **Table S3**. *BTU2* was used as a control. (C) *V-ATPase-a1* is required for

the mucocyst secretion. Cells were stimulated with dibucaine to induce mucocyst exocytosis. Centrifugation results in a dense pellet of cells with an overlaying flocculent comprised of the secreted mucocyst cargo. The flocculent layer is delineated with a solid at the upper border and a dashed line at the lower border. The *Δv-atpase-a1* cells are grossly deficient in mucocyst secretion and produce no apparent flocculent layer (right) compared to the wildtype (left). (D-E) V-ATPase-a1p is essential for mucocyst formation. (D) Docked mucocysts visualized in fixed wild-type cells by anti-Grl3p mAb 5E9 (top panel i), and anti-Grt1p mAb 4D11 (lower panel iii). *Δv-atpase-a1* cells contain less mucocyst signal and the Grl3p puncta are often irregularly shaped (top ii and lower panel iv). Inset shows single docked mucocyst. Scale bars, 10 µm. (E) Electron micrographs show mucocysts in both wild-type (top) and *Δv-atpase-a1* (bottom). In wild-type, immature mucocysts (labelled with blue asterisks) and docked mature mucocysts (labelled with red asterisks) are present. In *Δv-atpase-a1*, no mature mucocysts are present. The inset displays a magnified view of the selected field. Scale bars, 2 µm. (F-G) V-ATPase-a1p is required for processing of proGrl proteins. Cell lysates (5000 cell equivalents in F and 10,000 cell equivalents in G) were separated by SDS-PAGE and Western blotted using antibodies against Grl1p and Grl3p. (F) Western blotting using rabbit anti-Grl1p antibody. The mature processed Gr1p product predominates in wild-type cells, while the unprocessed precursor of Grl1p predominates in *Δv-atpase-a1* cells. (G) Same as F but using anti-Grl3p antibody. Lane L1: WT and lane L2: *Δv-atpase-a1*.

Figure 7. The *Δv-atpase-a1* cells show defects in vesicle trafficking during mucocyst biogenesis, similar to those in *Δvps8a* cells. (A) Wild-type (top panel), *Δv-atpase-a1* (middle panel) and *Δvps8a* (bottom panel) cells were double stained with rabbit anti-Grl1 and mouse monoclonal anti-Grt1 (4D11). Co-localization of Grl1p and Grt1p is significantly reduced in *Δv-atpase-a1* and *Δvps8a*, compared to wild-type. Optical cross sections are shown as single slices, for clarity. Scale bars, 10 µm. (B) Percentage of overlap (Mander's coefficient) between Grl1p and Grt1p using a sample of 26 non-overlapping images. The error bars show the SDs. (C) Wild-type (top panel) and *Δv-atpase-a1* (bottom panel) expressing Stx7l1p-GFP were double stained with rabbit anti-GFP and mouse monoclonal anti-Grt1(4D11) antibodies. In *Δv-atpase-a1* cells, there is a significant decrease in the co-localization of Stx7l1p and Grt1p. Inset shows co-localization between Stx7l1p and Grt1p. (D) A sample of ten non-overlapping fields was analyzed to determine the percentage of overlap (Mander's coefficient) between Stx7l1p and Grt1p using the Fiji-JACoP plugin. (E) Wild-type (left panel) and *Δv-atpase-a1* (right panel) cells expressing Sor4p-GFP were double stained with rabbit anti-GFP and mouse monoclonal anti-Grt1 antibodies. (F) The Fiji-JACoP plugin was used to calculate the percentage of overlap (Mander's coefficient) between Sor4p and Grt1p as before. Scale bars, 10 µm. The difference in cell size between samples is due to variable flattening by the coverslips.

Figure 8. Proposed model for the mucocyst biogenesis pathway in *T. thermophila*, extending that proposed by Sparvoli et al., 2018. Vps8ap and Stx7l1p are required for homotypic and/or heterotypic fusion of vesicles bearing pro-Grls and other mucocyst cargo proteins, to generate immature mucocysts whose subsequent maturation depends on processing enzymes and the AP-3 adaptor. We now include V-ATPase-a1 in this model, which appears to be required for the same step of efficient vesicle fusion to form immature mucocysts. These are transiently acidified, and subsequently Vma subunits are lost via V-ATPase complex disassembly during mucocyst maturation. At the end of this process, the mature docked mucocysts are non-acidic. The disassembly of the V-ATPase holo-complex appears dependent on AP-3, since the immature mucocysts that accumulate in Δ*apm3* are acidified.

Keywords

LRO, Mucocyst, V-ATPase-a1p, V-ATPase, pHluorin, VPS8ap, Rab7, Secretion, Exocytosis, AP-3

Abbreviation

LRO: Lysosome-related organelle, DCG: Dense core granule, GFP: Green fluorescent protein, V-ATPase: Vacuolar-ATPase, SEP: Super-ecliptic pHluorin, Igr1: Induced during granule regeneration 1, Vps8: Vacuolar protein sorting 8, Stx7l1: Syntaxin 7-like 1, Grl: Granule lattice, Grt: Granule tip, AP-3: Adaptor protein complex-3, VMA: Vacuolar Membrane Atpase

Fig1

A

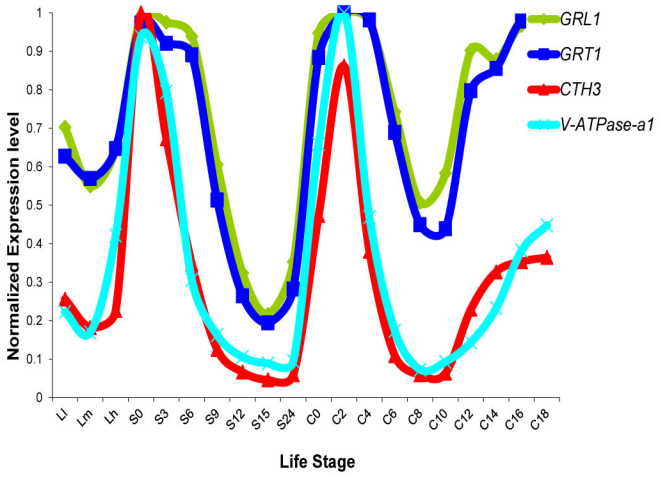
GRL1
GRT1
CTH3
V-ATPase-a1
Normalized Expression level
0
0.1
0.2
0.3
0.4
0.5
0.6
0.7
0.8
0.9
1
LI Lm Lh S0 S3 S6 S9 S12 S15 S24 C0 C2 C4 C6 C8 C10 C12 C14 C16 C18
Life Stage

B

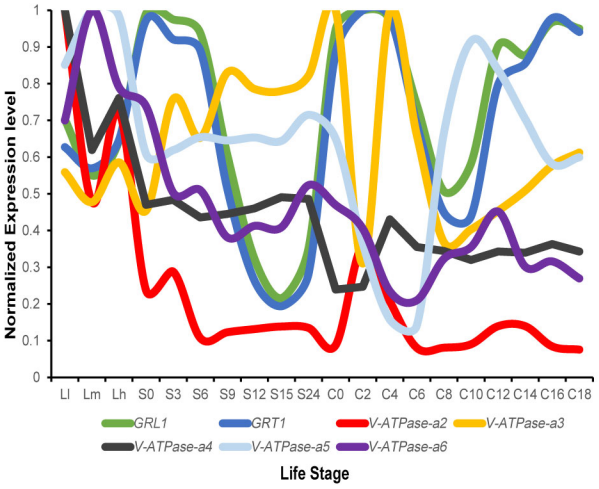
Normalized Expression level
0
0.1
0.2
0.3
0.4
0.5
0.6
0.7
0.8
0.9
1
LI Lm Lh S0 S3 S6 S9 S12 S15 S24 C0 C2 C4 C6 C8 C10 C12 C14 C16 C18
GRL1
GRT1
V-ATPase-a2
V-ATPase-a3
V-ATPase-a4
V-ATPase-a5
V-ATPase-a6
Life Stage

C

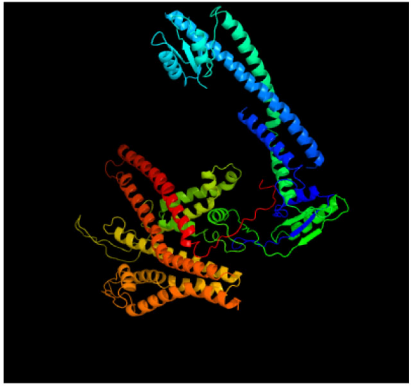

D

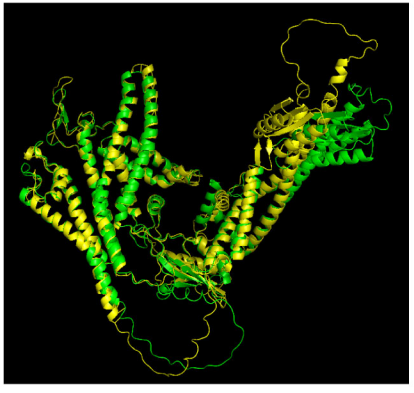

E

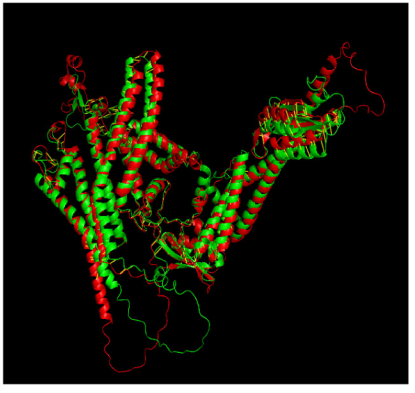

Fig2

A

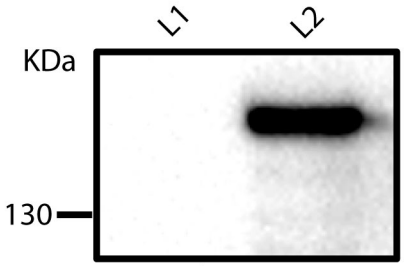

IP and IB: anti myc
L1: Cu428, L2: V-ATPase-a1p

B

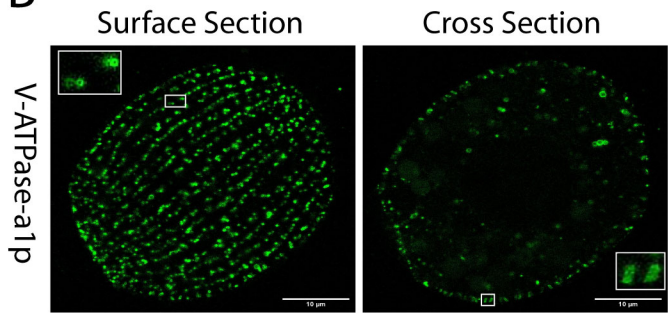

C

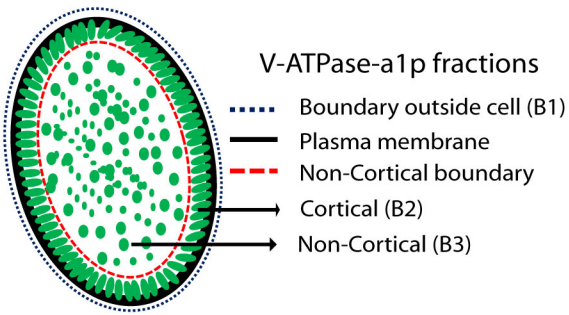

D

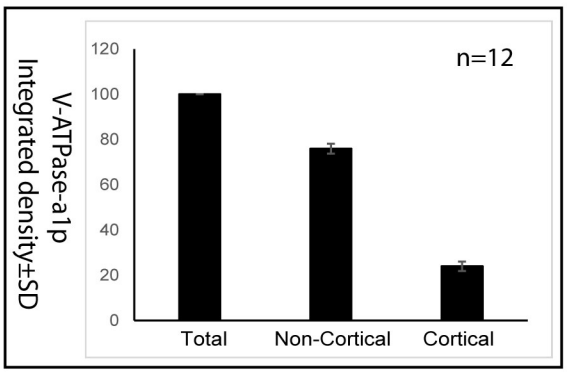

E

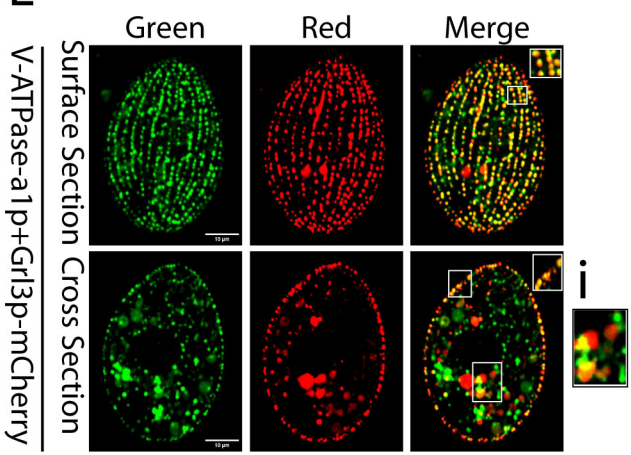

F

V-ATPase-a1p overlapping with Grl3p

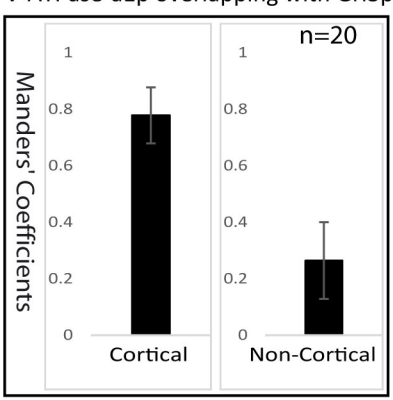

G

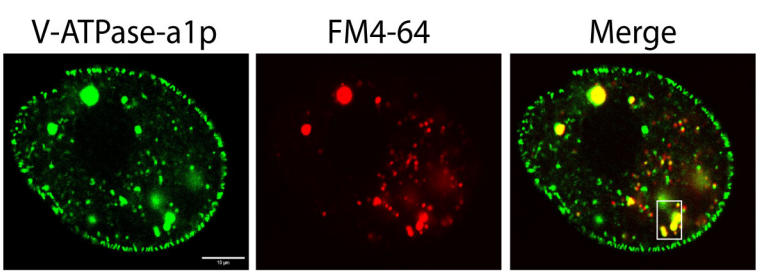

H

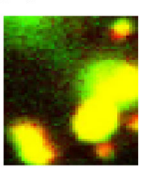

I

V-ATPase-a1p overlapping with FM4-64

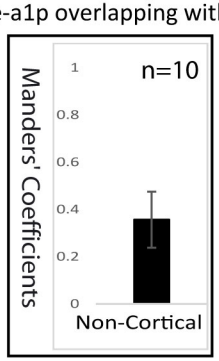

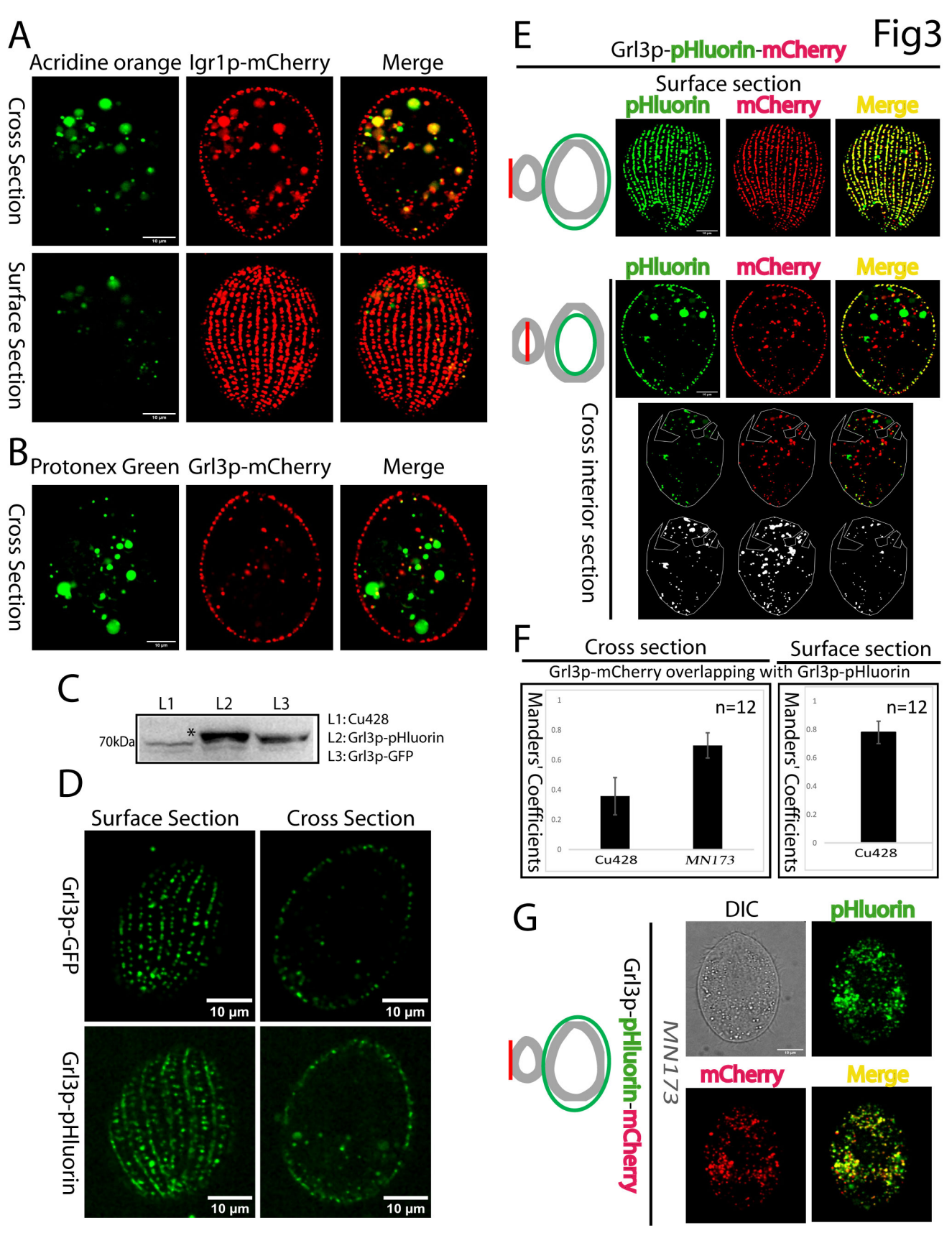
Fig3
A
Acridine orange
Igr1p-mCherry
Merge
Cross Section
Surface Section
B
Protonex Green
Grl3p-mCherry
Merge
Cross Section
C
L1
L2
L3
70kDa
*
L1: Cu428
L2: Grl3p-pHluorin
L3: Grl3p-GFP
D
Surface Section
Cross Section
Grl3p-GFP
Grl3p-pHluorin
10 µm
E
Grl3p-pHluorin-mCherry
Surface section
pHluorin
mCherry
Merge
Cross interior section
F
Cross section
Surface section
Grl3p-mCherry overlapping with Grl3p-pHluorin
Manders' Coefficients
n=12
Cu428
MN173
G
Grl3p-pHluorin-mCherry
MN173
DIC
pHluorin
mCherry
Merge

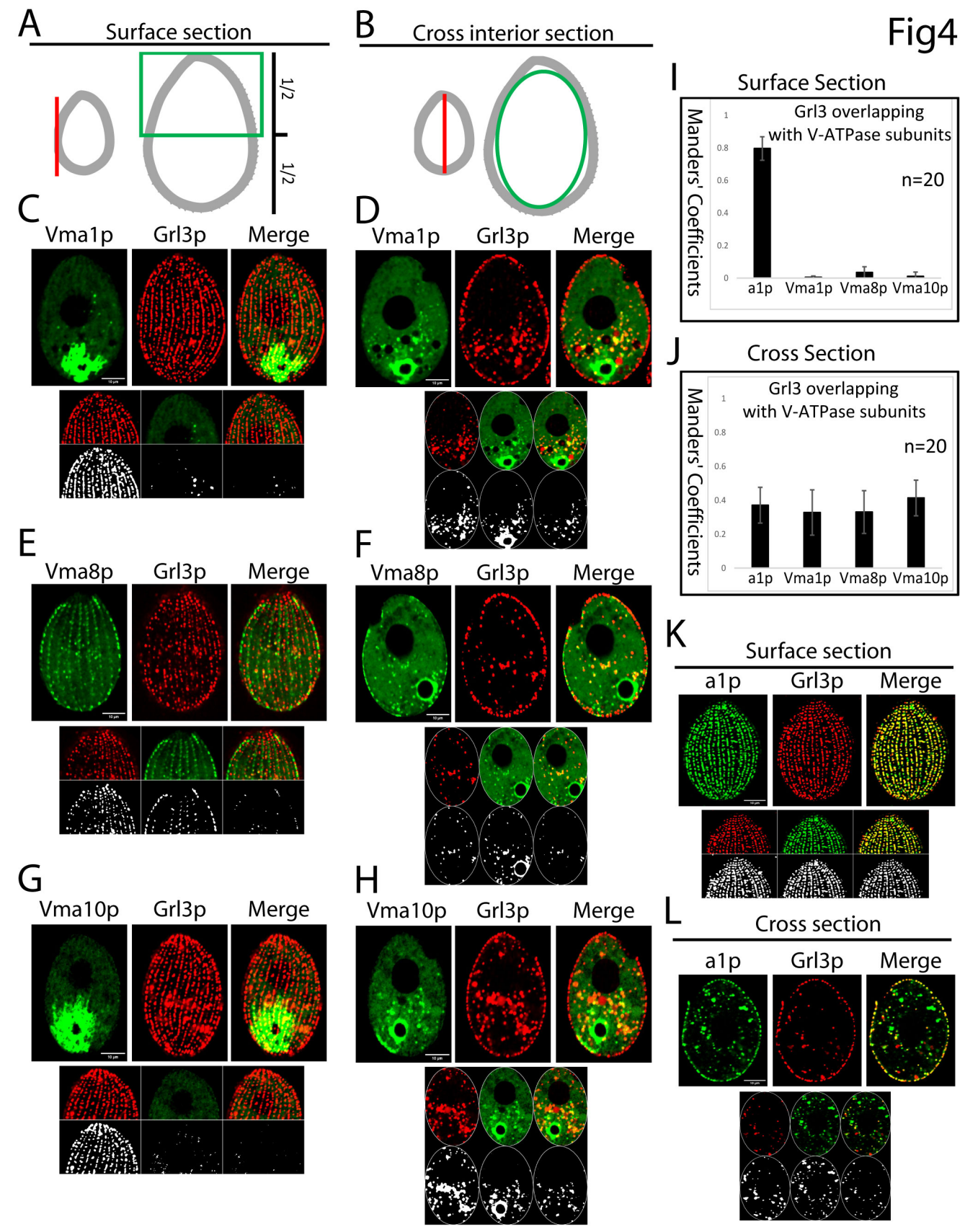
Fig4
A
Surface section
1/2
1/2
B
Cross interior section
C
Vma1p
Grl3p
Merge
D
Vma1p
Grl3p
Merge
E
Vma8p
Grl3p
Merge
F
Vma8p
Grl3p
Merge
G
Vma10p
Grl3p
Merge
H
Vma10p
Grl3p
Merge
I
Surface Section
Grl3 overlapping
with V-ATPase subunits
n=20
Manders' Coefficients
1
0.8
0.6
0.4
0.2
0
a1p
Vma1p
Vma8p
Vma10p
J
Cross Section
Grl3 overlapping
with V-ATPase subunits
n=20
Manders' Coefficients
1
0.8
0.6
0.4
0.2
0
a1p
Vma1p
Vma8p
Vma10p
K
Surface section
a1p
Grl3p
Merge
L
Cross section
a1p
Grl3p
Merge

Fig5

A

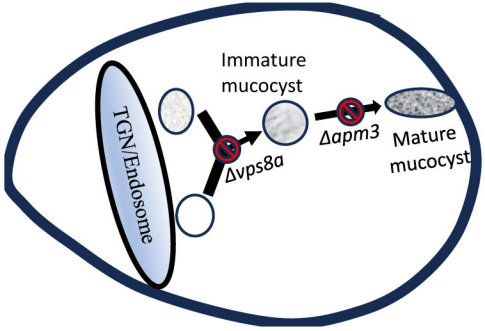

C

Grl3p-mCherry overlapping with Grl3p-pHluorin

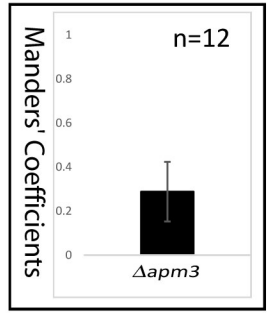

D

Grl3p-pHluorin-mCherry fluorescent puncta/cell

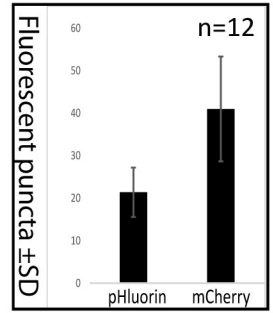

B

Grl3p-pHluorin-mCherry (Cross Section)

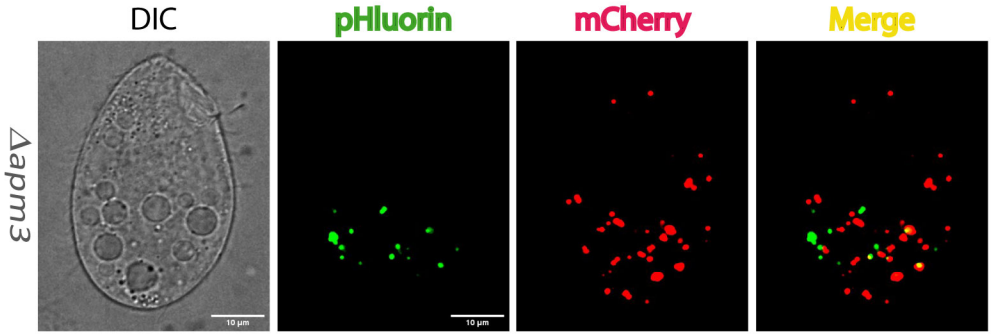

Fig6

A

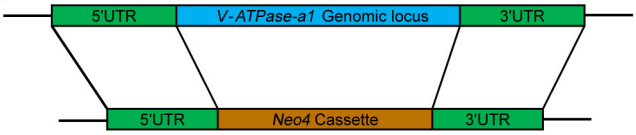

B

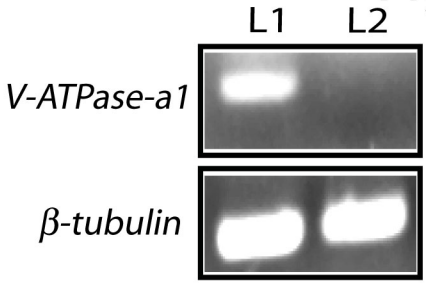

L1: WT, L2: Δv-atpase-a1

C

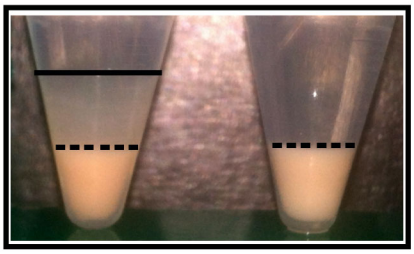

D

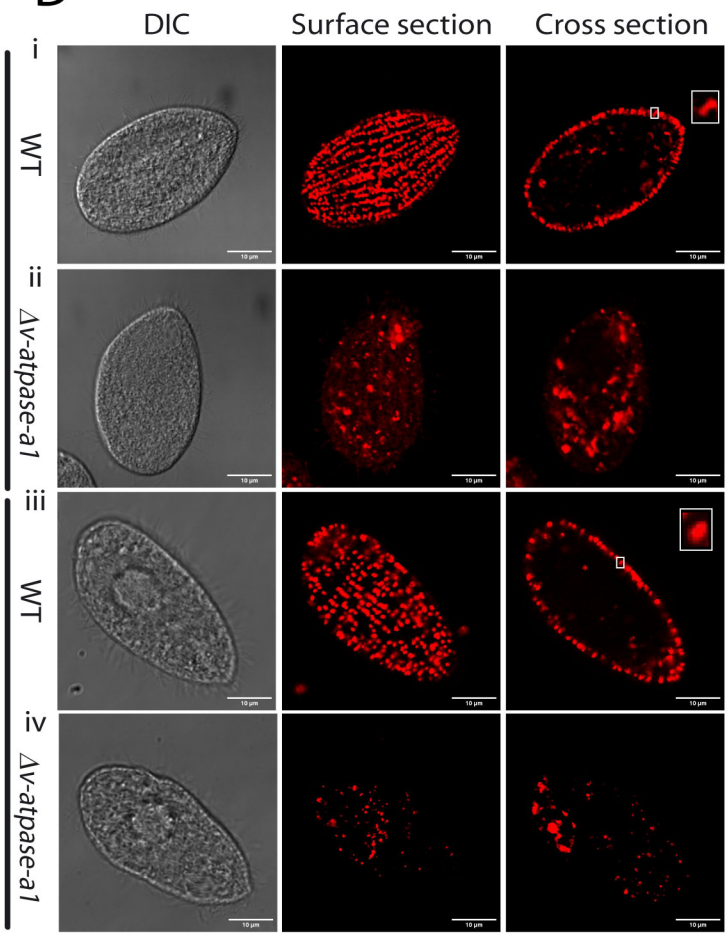

E

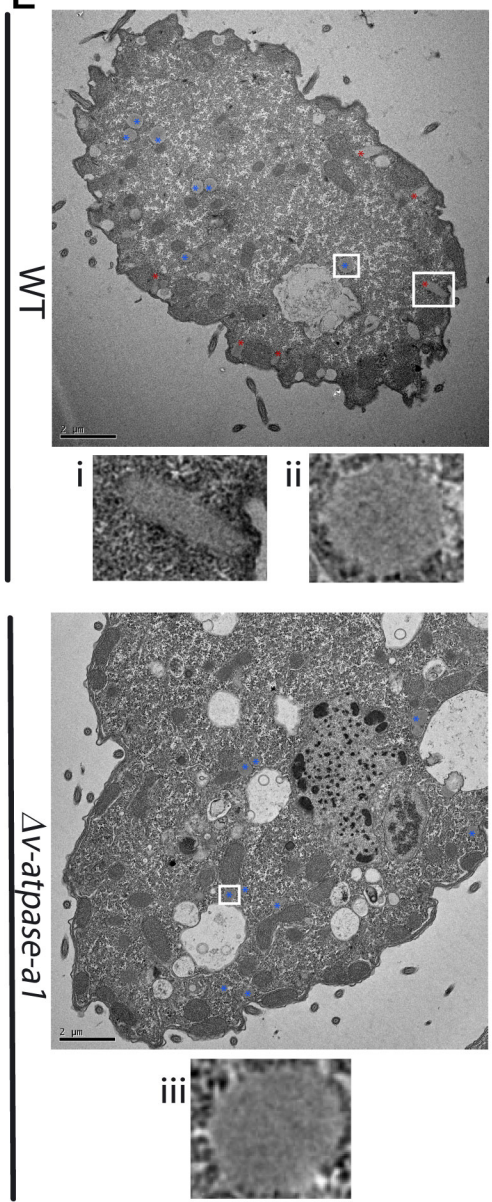

F

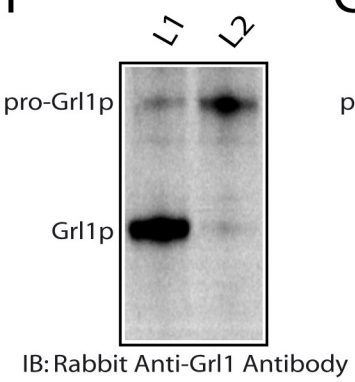

IB: Rabbit Anti-Grl1 Antibody

G

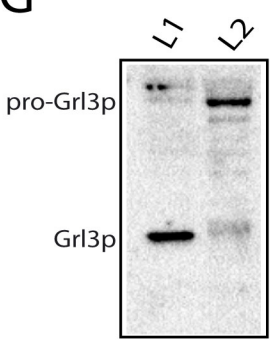

IB: Rabbit Anti-Grl3 Antibody

Fig7

A

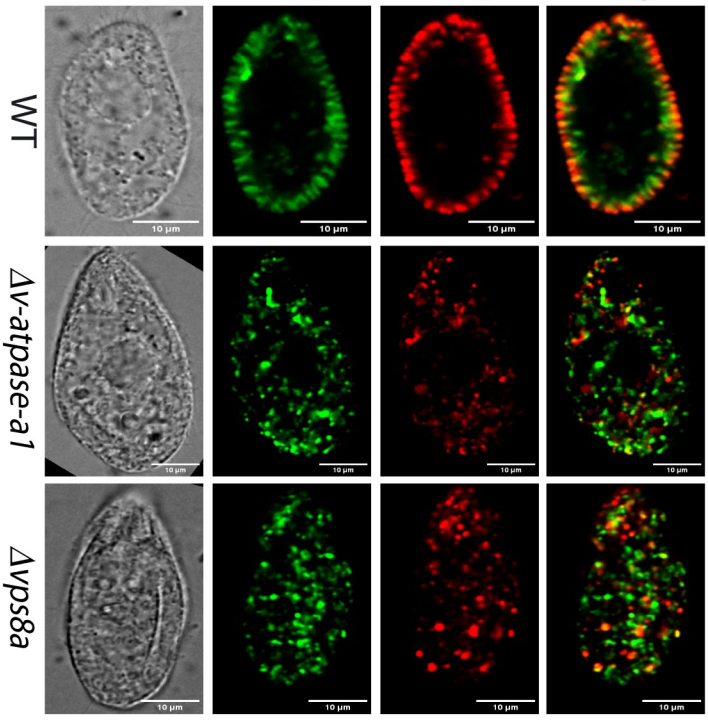
DIC
Grl1p
Grt1p
Merge
WT
Δv-atpase-a1
Δvps8a
10 µm

B

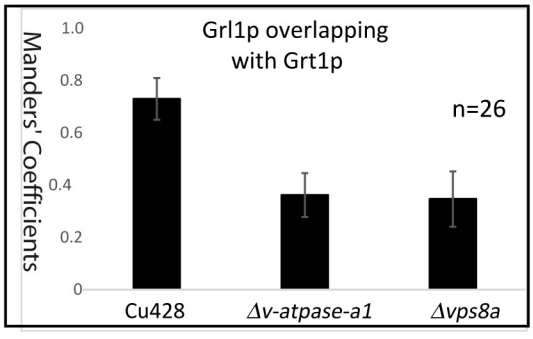
Grl1p overlapping with Grt1p
n=26
Manders' Coefficients
1.0
0.8
0.6
0.4
0.2
0
Cu428
Δv-atpase-a1
Δvps8a

C

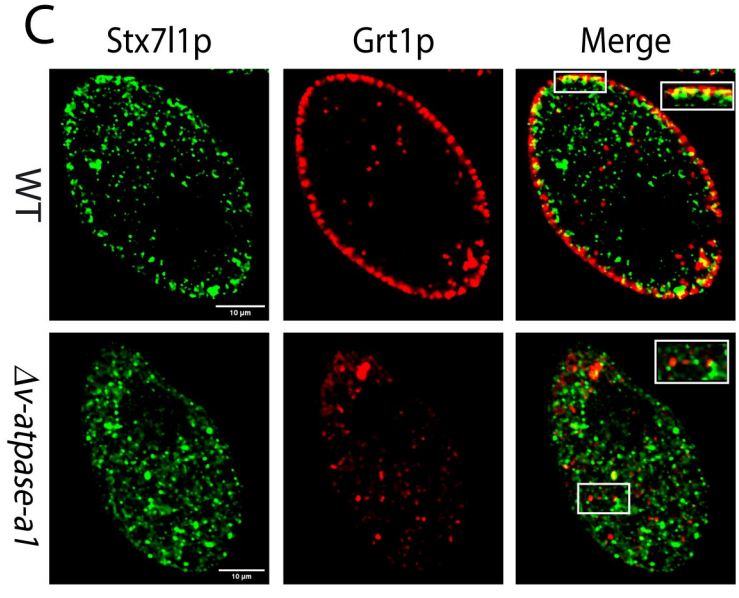
Stx7l1p
Grt1p
Merge
WT
Δv-atpase-a1
10 µm

D

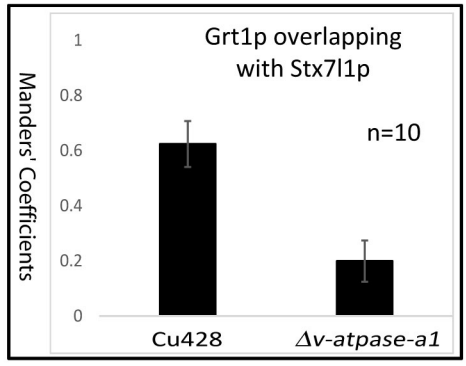
Grt1p overlapping with Stx7l1p
n=10
Manders' Coefficients
1
0.8
0.6
0.4
0.2
0
Cu428
Δv-atpase-a1

E

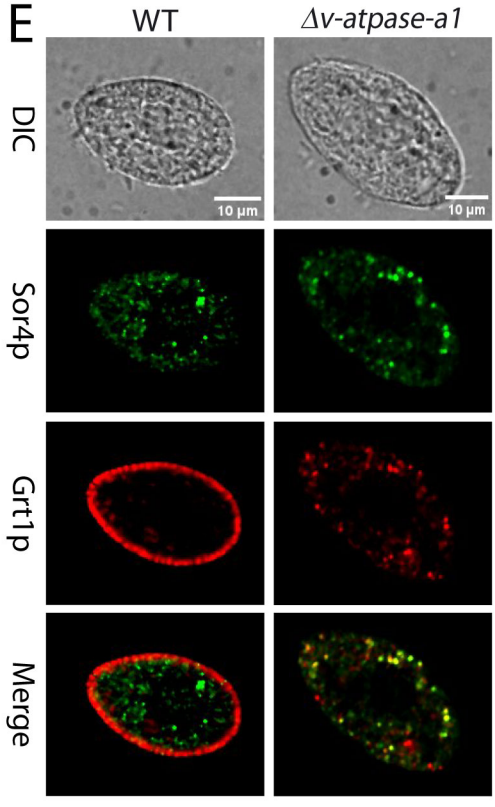
WT
Δv-atpase-a1
DIC
Sor4p
Grt1p
Merge
10 µm

F

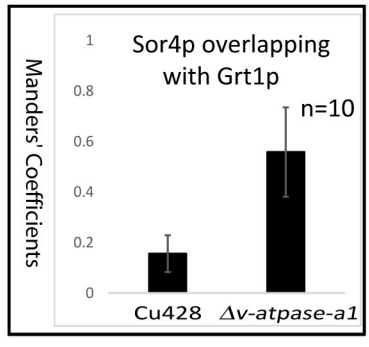
Sor4p overlapping with Grt1p
n=10
Manders' Coefficients
1
0.8
0.6
0.4
0.2
0
Cu428
Δv-atpase-a1

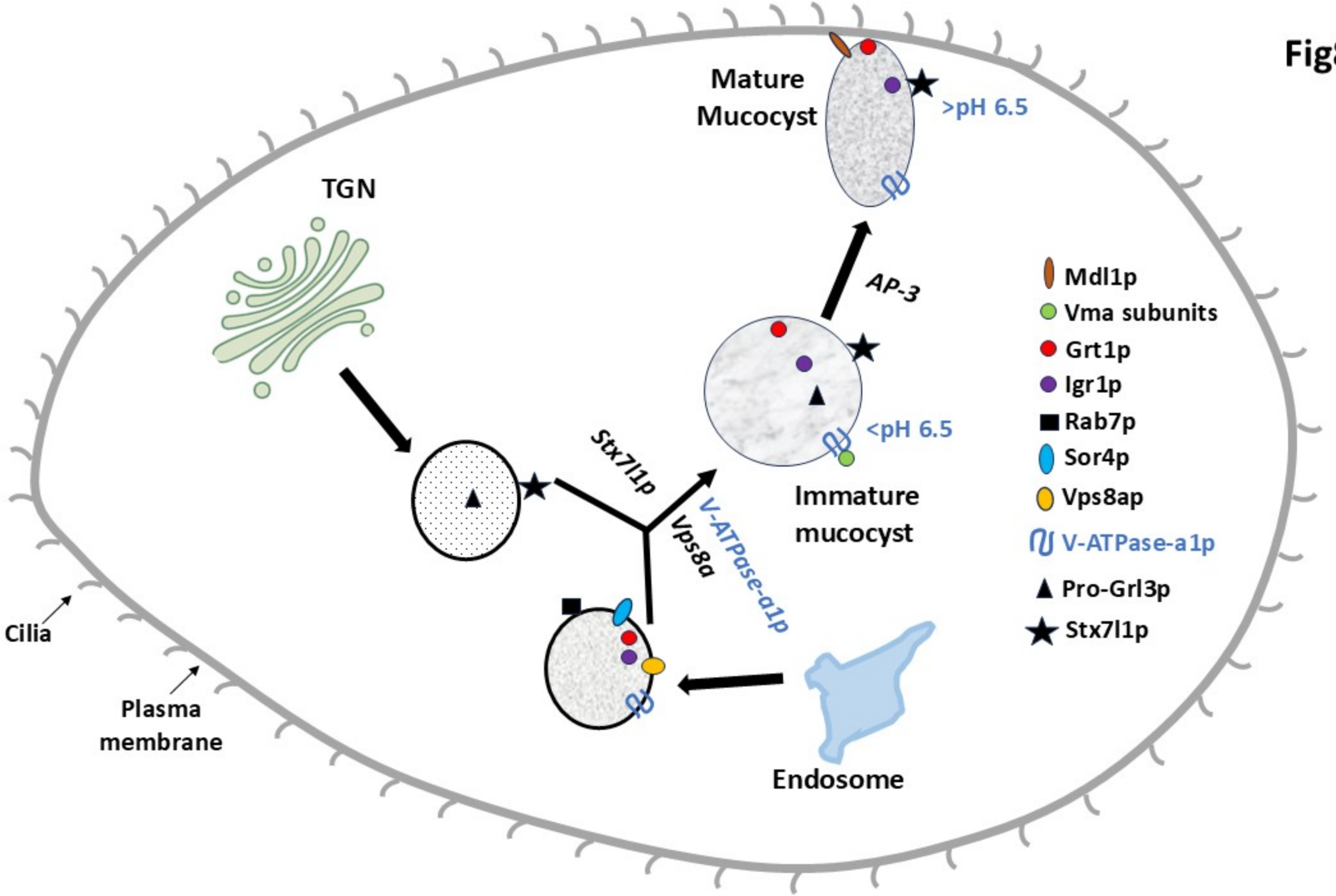
Fig8
Mature
Mucocyst
>pH 6.5
TGN
AP-3
Mdl1p
Vma subunits
Grt1p
Igr1p
Rab7p
Sor4p
Vps8ap
V-ATPase-a1p
Pro-Grl3p
Stx7l1p
<pH 6.5
Stx7l1p
V-ATPase-a1p
Vps8a
Immature
mucocyst
Cilia
Plasma
membrane
Endosome

FigS1

```
V-ATPase-a5/1-915   1 MRQKVQRIQIKQKIKIKQNQEIKNIKNYQAKQRGNKQTINQAKQQNKEDRKQKKYKKTTEKMSLLRSDKMAYYNIVIPRESAWEVLN  87
V-ATPase-a6/1-912   1 ------------------------------------------------------------MLRSERMGCYQVIVSRELAWEMIN  24
V-ATPase-a3/1-877   1 ------------------------------------------------------------MSLFRSEDMEYCRIVLPRESAWETLN  26
V-ATPase-a4/1-924   1 ------------------------------------------------------------MNIFRSENMGYYHLILPRESSWEVMN  26
V-ATPase-a1/1-839   1 ------------------------------------------------------------MGSFFRSEEMELYCLLIPRENSYNLVS  27
V-ATPase-a2/1-859   1 ------------------------------------------------------------MLRSEKMSLHCLLMPRESAWEVLN  24

V-ATPase-a5/1-915  88 QLGQV--QVVQFEDQNAHESHMSRVFTPQIKRAEDILNQIHIIHNLMVAKQ----KEVTK--------CDNIQAYLD-VLEVYLRGR 159
V-ATPase-a6/1-912  25 MLGELGDDMVEFIDSNKDQNSANRLFSRFIKKCEEIQTNLAKIKQLLKDYN----FHIQH--------CEDVEEFLI-QLREFLSTR  98
V-ATPase-a3/1-877  27 ELGKN--DCIHQVDTDSLLPNIARPFHNQIKRCDEVEFMLNDIKGYINKYE----GLIIK--------CKNIKELVEVVFPKVLDIR  99
V-ATPase-a4/1-924  27 ELGGL--SLLHFIDQNPDLPNVNKAFTNYIKRCDEVLFKLNLIKKQMQNFD----KEINK--------PDNFKDLQG-YFNKILQER  98
V-ATPase-a1/1-839  28 SLGDK--DLFHFIDAEPHIPQFTRLYSKQTKRCDELLSKIDEIGQIMNQFG--YDHGLGK--------GDVTNFLN-LLEIKKKSR 100
V-ATPase-a2/1-859  25 DLGTL--DKVHFVDCEEDVPQFNRPFYQQVRRCDESLQKLLWIENEMQKFYNFYNQVIKSNNQVNIDYCGDLASFHE-YLKKDVESR 108

V-ATPase-a5/1-915 160 EKAYHTFIDDVESQVKDAFAKLNEQTFTLESLTSKYYSLIEYSNVLRKFKEKVVD----------------QRIMSGLDN-------- 223
V-ATPase-a6/1-912  99 DRIEKTYIDDINQEIESFTKQIFRNAAQVEELEKKYQDLKEQSSTYLFYKDRFISSLYYQHREDLERKKKQKLQSQIQNVEEIEQET 185
V-ATPase-a3/1-877 100 QRAGKTYFEEIENDVIQRYNNLKDQIQNLDNISEKQKQLEEYKQVLNNAQAIMGDAFFMDQK--------QSQSD------------ 166
V-ATPase-a4/1-924  99 EKAGQTYFEEIEDSVYQKATQLEEQINNYTNLQDKQDHLVEYKDVLIKAKTILGPSFFKNQQEIDEEASIQSVQESVSGL------- 178
V-ATPase-a1/1-839 101 KQDEQYYIDELEKEIKTVLVDIQKQIAAAHKTRMNMNLLVEQIVCLEKIVPLITGD--------------QQIPS------------ 161
V-ATPase-a2/1-859 109 RINEQAYFLQIENEINQKHKFLEQLIHNFNSVITYRNQLVEKKHVLTEASRVLNVN--------------QLNQD------------ 169

V-ATPase-a5/1-915 224 --------IAINPLELAEEGKEE----ENP----LASASKLFYITGTINKEDTLRFKKIIFRTTKGNSWVFTS------EIPYDQGE 288
V-ATPase-a6/1-912 186 VVVLSSKPVSRRQQPIQQKHRNE----EDADWEDQFLTRQFTTVIGTVKTEDIYRFIRSIYRLTKGNFWN----------IQKVHAE 258
V-ATPase-a3/1-877 167 ------EKIDIHGKGL----------------EELKSDFNLNKISGIIDTSDVNRFQKFIFRITKGNCFIAFK-----EAQELST-- 224
V-ATPase-a4/1-924 179 ------QQIDINQSQLSLAMRDMNIPLQKHHGINIESNLKLNYVVGTVSDSDAAKFQKTIFRITKGNSWVIMQNLEQKQQNEVSANV 259
V-ATPase-a1/1-839 162 ----------FSSL-------------------SEDQSRIGKIIGTINMSDSLRFQKSMFRATKGKCFIYAQ------PIETTGTK 212
V-ATPase-a2/1-859 170 ----------NQIP--------------------NPDRVSLNFLAGVINADDEVRFHKSAFRVSRGNIWKHFK------QIDKSMQR 220

V-ATPase-a5/1-915 289 ---------------------FKEGFQKSVFIVAFSGG-SGVLKSKLNRVCDSFNASKYSMPRDPNGYNSKFLEIQQQISDTRQLMR 353
V-ATPase-a6/1-912 259 ---------------------FPDRTIFILFFPVASIQ-NSYLIGKINKILDVFNAKIFKSIINKDEIDLKILQIEQDKTDVLRVIN 323
V-ATPase-a3/1-877 225 ---------------------LHSQSRSVFVLMFPGNRNGLVYQKASRICESFNANRFQCPSNQTEFNQKLAEIDRQIIEGKQIIN 289
V-ATPase-a4/1-924 260 ---------------------MPQKVGRSVFLMLIPGQQAGFINQKIQRICDSFGVNKYQFPETPDKYEKRLQDLDNQIRDSRHLLK 325
V-ATPase-a1/1-839 213 --YKIVNPD-----------NPNEEIKKGVFLFIYN--QSSLLEAKLMRICQSVEANVFKLEGDEENLQLDIQQNAEDYQKSKELLR 284
V-ATPase-a2/1-859 221 DGYKLLNIKGQRDHDTSELTDPYNSVQKTIFILAYASGQNSSLDRKLRRICEGFHADVFNIQYS--NISKDLKETEEQIRNQNLTVQ 305

V-ATPase-a5/1-915 354 LTENALNNVLDEWIQ-------PRIGNQCSYIEELRLFVVKEKYIYTNMNMLTVKS-AVFGGYFWCPEEQDHAVLKAIDKVR-TNNP 431
V-ATPase-a6/1-912 324 LAKKQLYSDLEEWSL-------PRKGLNCSKIVEMQLFVEKERSIFVQLNNLKPRK-HVFIGRLWCPKVYQEQLLQTQVKLS-LKYP 401
V-ATPase-a3/1-877 290 LTKKNLISYLEEFTV-------VKHNAGCSYVEYLNCYVAKERRIYQAMNCLRISG-SVLVGFCWVPTEKVPDAQYALGQLA-NKYS 367
V-ATPase-a4/1-924 326 LTQREINDFLETFSQ-------NRNDCKCSYIEELIYYIEKEKLLYTNLNYLKAQS-THYHGNCWLPKDEEESILKALQNIR-LRYP 403
V-ATPase-a1/1-839 285 LTYKHLEQIFSRLQ--------DQTEEIT-LLEQYRLHLVREKQIYHHIN-LTKNTGAVLKAYVWLPKSEEESVIQFLQSSQDPRYA 361
V-ATPase-a2/1-859 306 LSEKSINEYFDFYQKSIKLQSGDQVVDVCSYIEYVRLFLHKEKTIQHNLNYLVQSSQTFCKGLIWVPEEDEGIVQRRVEQLTQKKSN 392

V-ATPase-a5/1-915 432 NIGMTEVKK---QERPSHLEPPTHFRTNDVTAPFQEIVNTYGIPRYREVNPGLFCISMFPLKFGIMFGDIGHGGALFAFGAWLVYKG 515
V-ATPase-a6/1-912 402 NQGQSQIIE---CEINDDDVPPTLFKLNSFTAPFQQIVNTYGIPRYKEINPGIYCIVMFSLQFGIMFGDIGHGGFLFLFGLYLCINH 485
V-ATPase-a3/1-877 368 NLPSSTLKV---ISAGDQ-KPPTYFKLNDFKAVFQTIVDTYGVPRYKEVNPGLFTIVTFPFLFGVMFGDIGHGGLLFIFGLYLLFFK 450
V-ATPase-a4/1-924 404 HLPNGQLQE---VIPAAG-VPPTYFKLNDFTRVFQVIVNTYGVPRYKEVNPGLFTIVTFPFLFGVMFGDIGHGFLLFVIGCYLCLWK 486
V-ATPase-a1/1-839 362 TAQLHPVSTSDYSKLTIENKRPTKIEKNQFLDVFQEIINTYGIPRYREINPGFFSIITFPFLFGVMFGDIGHGILLFTYGCYL--MS 446
V-ATPase-a2/1-859 393 SVQVAQLYK--LSNYTIDP--PTKFKSNDFTIPFQEIVNTYGIPRYREINPALFAISTFPYLFGMMFGDIGHGALLFTIGLYL--MS 473

V-ATPase-a5/1-915 516 KE-LLNTP--LAALFPARYLLALMGLFAFYCGLIYNDFLALPINLFG-SCYYN----VHHDGEVHEGQAHYTIEKHENCVYPLGFDP 594
V-ATPase-a6/1-912 486 KKNPFDTRRDLNVLYSVRYVVLLLGFFALYSGLIYNDFFSLPIYLFHKSCYVN----QRDE----NGELEY--VKKPNCTYPFGFDP 562
V-ATPase-a3/1-877 451 DSILNDKFSSIKALIPARYIIVLMGFFALFCGFIYNDFLSLRLDLFG-SCFQVNTKTVTDPKTQQQMQEEYVIPKSRDCTYPFGIDP 536
V-ATPase-a4/1-924 487 EKIENDPSSTFKLMLPARYIIIMMGFFATFCGLIYNEFFSIVFNIFG-SCYNL----------EEINGTQTITKIPDCVYDFGFDP 561
V-ATPase-a1/1-839 447 T--YDKKLHHEDQLYKCRYIISMMGFFAIFCGFIYNDFMSIPLDLFG-SCYTF----------QGK---SKLKRKDECVYPFGMDP 516
V-ATPase-a2/1-859 474 CKIDPKRPSAMDGLVQARYLITLMGLFALYNGLIYNDFMSLPLNLFG-SCYLL----------ADKNVVLTHKTSKQCVYPFGIDP 548

V-ATPase-a5/1-915 595 KWYISNNELNFFNSFKMKFAVIFGVAQMSWGIFLKGLNCIHFDLWVDLIFEWLPQMVFLLSTFGYMCFMIIFKWVSQYEEG------ 675
V-ATPase-a6/1-912 563 KWYIAQNELTFFNSFKMKLAVIIGVIQMTFGIILKGFNNKYFGQWIDFFFEFIPQLVFMVTTFGYMIFMIVIKWNINYQQDT----- 644
V-ATPase-a3/1-877 537 MWGKTSNELTFVNSFKMKLAVIFAITQMCLGISMKAFNSVYFKKWVDFFFEFVPQILFMGLMFGYMDYLIFAKWTIDYTDGEYNIPK 623
V-ATPase-a4/1-924 562 IWMLTSNNLTFQNSFKMKFAVIAIIHMSLGICMKAFNAIFFKSKADFYFEFLPQLLFLLTFGYMDFLIIIKWVQNWTQ---HILE 645
V-ATPase-a1/1-839 517 VWLDSQNSLTFFNSFKMKSAIILGVSQMLLGILLKGLNSMLQLSALDFFFEFLPQLLFFICTFGYMALLIIIKWLSSFAP------- 596
V-ATPase-a2/1-859 549 VWGVAKNKLSVYNSLKMKTSVVFGVFQMLIGIFLKGLNAINNISFVDFFFEFIPQVVFMCCTFGYMVFLIFMKWMTDYSQNT----- 630

V-ATPase-a5/1-915 676 -YLAPSIINQMINLPLKMGQVSTFNGTPTPLFNDS-KFQEELQYNLLIISVACVPIMLLIKPLFFLLKKK---------------- 743
V-ATPase-a6/1-912 645 -SQAPSIINLMINLPLKLGMIPDGK----SLWNQ--ENQEYLQQNLLYISVCMVPLMLFPKPFLLYLKNRKNNKRTYVVKKGSLNEK 724
V-ATPase-a3/1-877 624 DAKVPSIITMIDMALTLGN---VKSENGSIISN----QRTIQTIILVVSLLCVPMMLFPKPIILHLQNKRK-QRLSHIADDHSQ-- 700
V-ATPase-a4/1-924 646 ANPPPSIITLMINIPLKGADPAGAALFGPSDAGI----QKSIGIIFLLIAIVCVPIMLLPKPFIQNYINKKKHQALNGDLDDHNQDK 728
V-ATPase-a1/1-839 597 -SEAPSILTIMLNFILNFGKLDPNYDNILGYIDVSRKQQEKLQFYLLIVAAVCVPLMLFPKPIFQYLFGSSKSSEDQHIQSPQVLEIQ 682
V-ATPase-a2/1-859 631 -SKAPSILTYMLDLGLSGGG--------VGHQQELYKGQGVDQPYLLIAALISVPIMLLAKPIIHQMQHN--SHQQHQNAEGFVPFQ 706

V-ATPase-a5/1-915 744 --PQHQEVHDES-----------------EPLLQSHAPP-----------------------------SHDDHDFNEVFVHQV 778
V-ATPase-a6/1-912 725 LIPQLQKNQNSD------------------DDFIQELRKSQIEKEETIKKQFLKENSIQESMDFDQFESITKDKHEFDFSEVFVHQV 793
V-ATPase-a3/1-877 701 QHLLHGQDE--------------------DDLARDLEKAQLKLLNSG-IDSQKQGGGH--------------GEHEAFGEIFVHQI 751
V-ATPase-a4/1-924 729 KYLIREEHKSEISPRHDSQQGHNNLQEIPLDDLQKDLEYQSLKENIEIHHNVNNEQISDDHH----------IEVGEHEGFADLFVHQV 805
V-ATPase-a1/1-839 683 DQEEIQSQSQHH-------------------THHDKQHLKQQEQ-----------------------------HTSHESFSELFVHQV 722
V-ATPase-a2/1-859 707 D--DIEENRRQA------------------DNFIEKGLKLHKN-----------------------------EKPHE-FSEEFVHQV 743

V-ATPase-a5/1-915 779 IETIEFVLGSVSNTASYLRLWALSLAHGQLAKVFFEKTIGGGIVGGS---ALQIIIGWFLFLNISFAVLMCMDLMECFLHALRLQWQ 862
V-ATPase-a6/1-912 794 IETIEFVLGSISSTASYLRLWALSLAHSQLSKVFFEKTIGSGIIEGN---SLQIILGWFVFVHITVFLMSMDLMECFLHAIRLQW- 876
V-ATPase-a3/1-877 752 IETIEFILGSISNTASYLRLWALSLAHSQLAAVFFDKALKSGLENAN---IPMLVIGYLVFAKVTLGVLMAMDVMECFLHALRLHW- 834
V-ATPase-a4/1-924 806 IETIEFVLGSISNTASYLRLWALSLAHGQLSRVFFQKALQPFIIEMDGGVQIIALIIGYYVFALVTFGVLMCMDVMECFLHALRLHW- 891
V-ATPase-a1/1-839 723 IESIEFVLGSVSHTASYLRLWALSLAHSQLAHVFFEKTLQSSIENSS---ILGLLVGYFIFALITFGVLMCMDVMECFLHTLRLHW- 805
V-ATPase-a2/1-859 744 IETIEFVLGSISHTASYLRLWALSLAHSQLAEVFFEKTLKGQIESGS---TIGILVGFIVFAMITFAVLMCMDVMECFLHTLRLHW- 826

V-ATPase-a5/1-915 863 LLLQNFVLIDYQILKNLFRVEFQTKFYKADGYKFEPFSFVDALNRANEAEQAK--------- 915
V-ATPase-a6/1-912 877 ---------------------VEFQGKFYKADGVWFNSFSFLGNLRQFNVDLSNGIK-------- 912
V-ATPase-a3/1-877 835 ---------------------VEFQSKFYKADGYAFSPFSFVNAIKEAVPSEDDEAEAAKKQKQ 877
V-ATPase-a4/1-924 892 ---------------------VEFQSKFYKADGYAFVPYSIEKHFIELSQSKDA---------- 924
V-ATPase-a1/1-839 806 ---------------------VEFQSKFYKADGVTFQPLSFKTSLAQHQIYYENN---------- 839
V-ATPase-a2/1-859 827 ---------------------VEFQSKFYKADGYLFKPFSVNNVLSVAAVEKRY---------- 859
```

FigS2

A

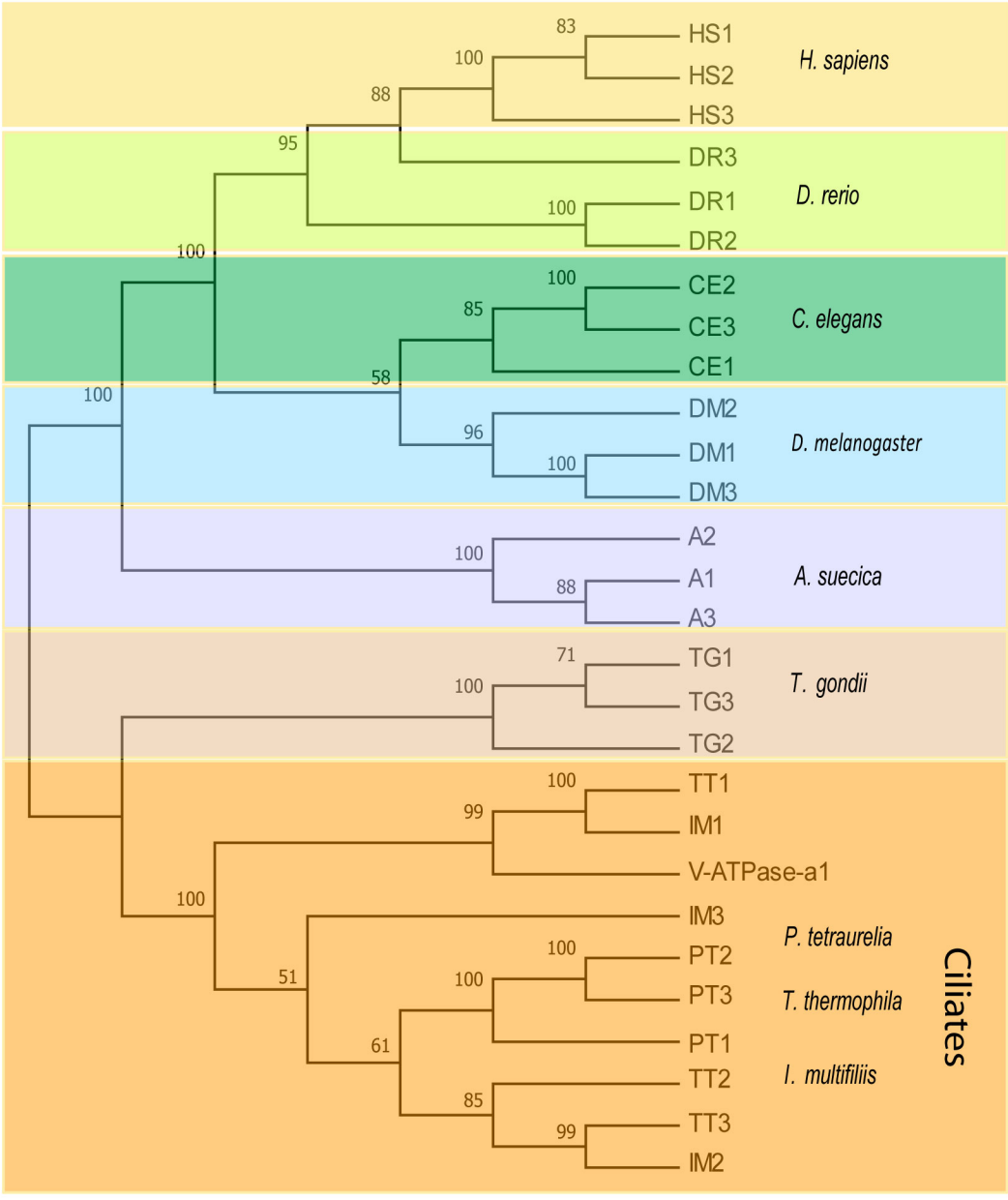
HS1
HS2
HS3
H. sapiens
DR3
DR1
DR2
D. rerio
CE2
CE3
CE1
C. elegans
DM2
DM1
DM3
D. melanogaster
A2
A1
A3
A. suecica
TG1
TG3
TG2
T. gondii
TT1
IM1
V-ATPase-a1
IM3
PT2
PT3
PT1
TT2
TT3
IM2
P. tetraurelia
T. thermophila
I. multifiliis
Ciliates
83
100
88
95
100
100
100
85
58
100
96
100
100
88
71
100
100
99
100
51
100
61
85
99

FigS3

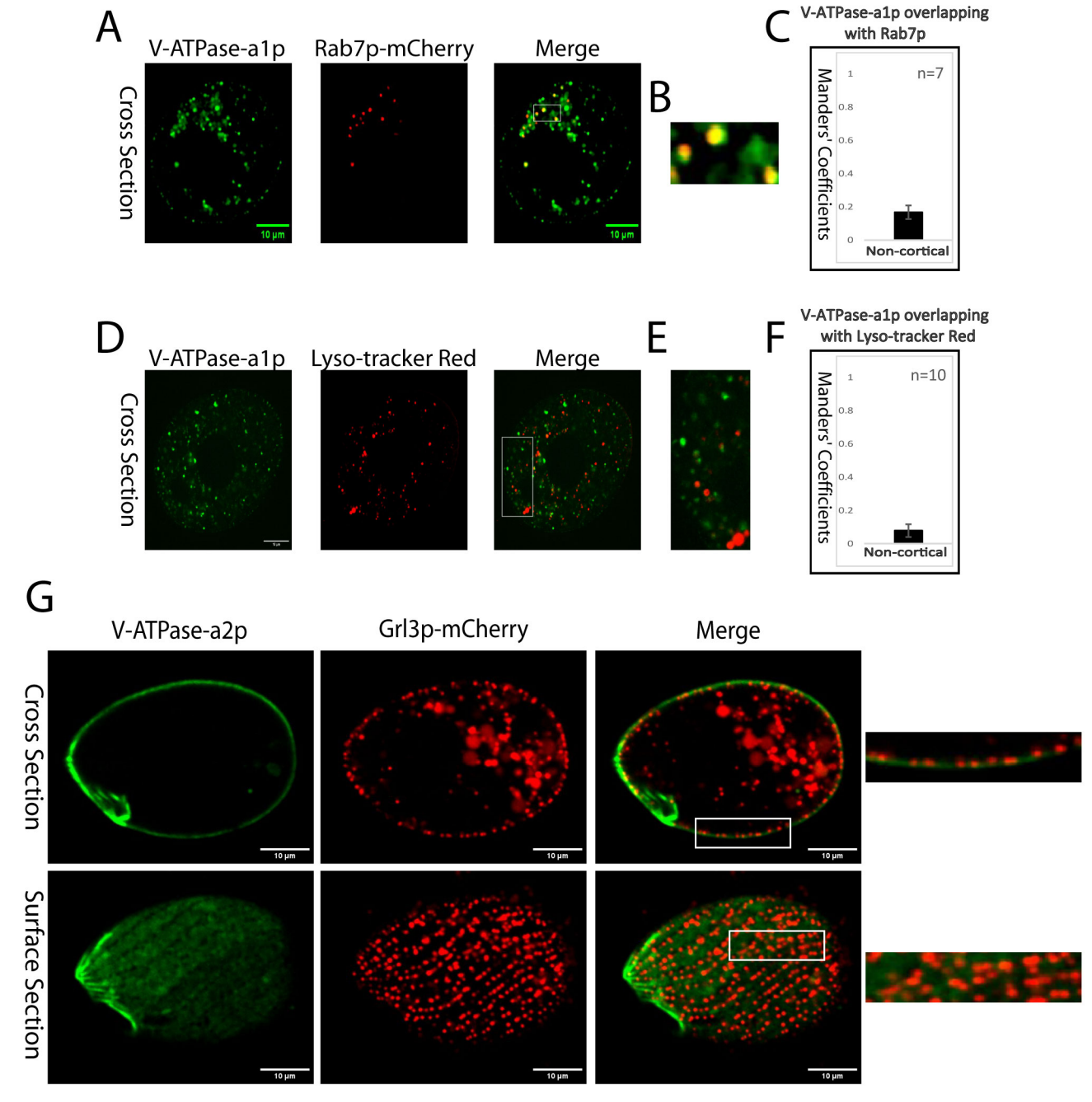
A
V-ATPase-a1p
Rab7p-mCherry
Merge
Cross Section
10 µm
B
C
V-ATPase-a1p overlapping with Rab7p
Manders' Coefficients
n=7
1
0.8
0.6
0.4
0.2
0
Non-cortical
D
V-ATPase-a1p
Lyso-tracker Red
Merge
Cross Section
E
F
V-ATPase-a1p overlapping with Lyso-tracker Red
Manders' Coefficients
n=10
1
0.8
0.6
0.4
0.2
0
Non-cortical
G
V-ATPase-a2p
Grl3p-mCherry
Merge
Cross Section
Surface Section
10 µm

FigS4

A

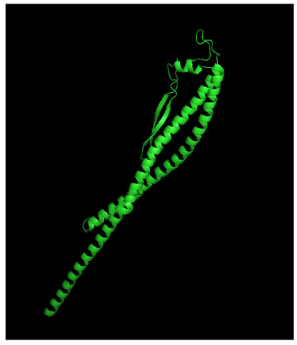

Vma8p

B

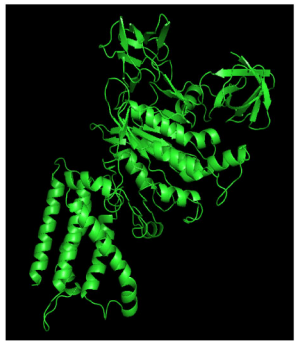

Vma1p

C

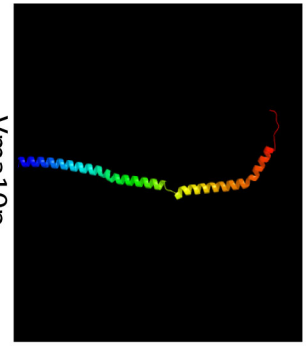

Vma10p

Confidence:: 100%
Coverage: 62%
% i.d.: 28%
Structural Homology with V-ATPase subunit-G of saccharomyces cerevisiae

D

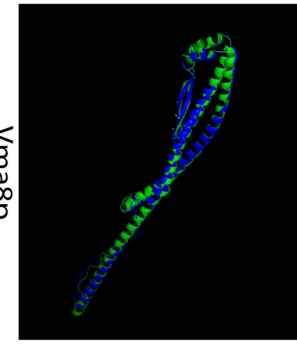

Vma8p

E

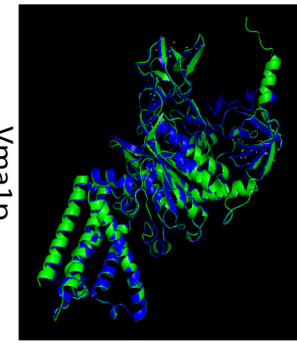

Vma1p

F

Grl3p-pHluorin-mCherry

DIC | pHluorin | mCherry | Merge

Δapm3

Cell 1

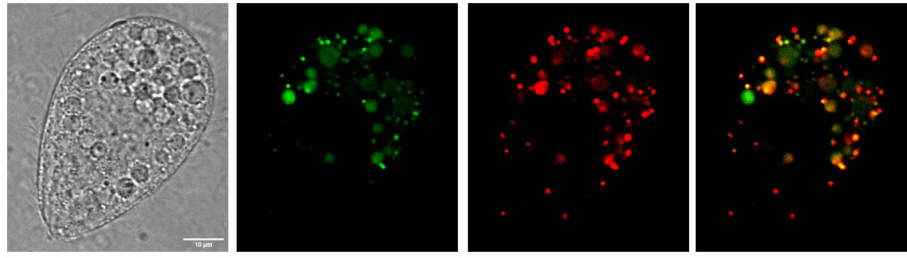

Cell 2

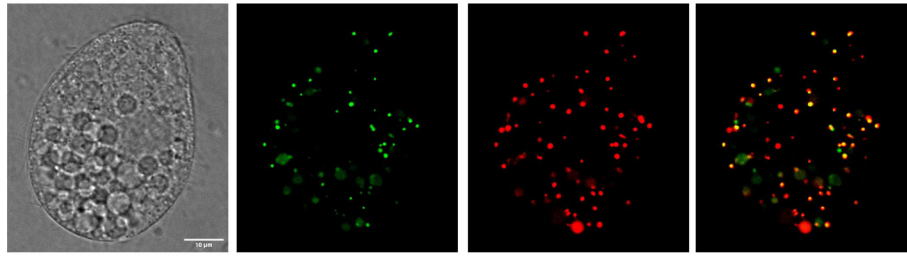

Cell 3

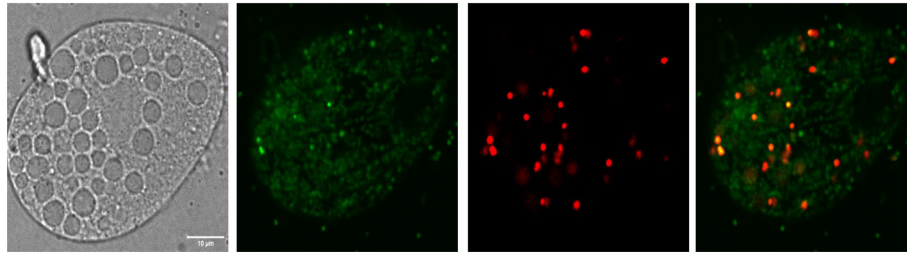

Fig S5

Δv-atpase-a1

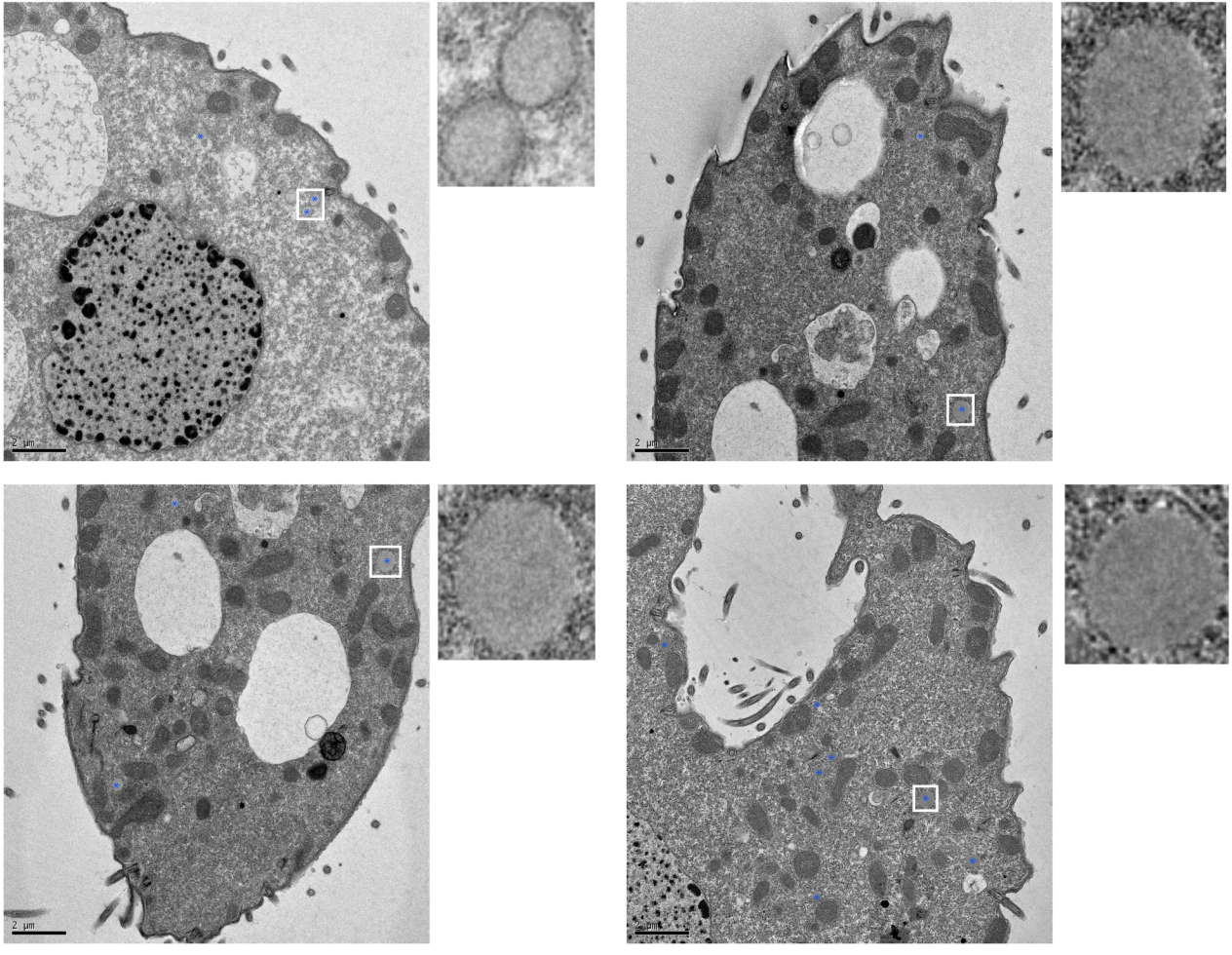

FigS6

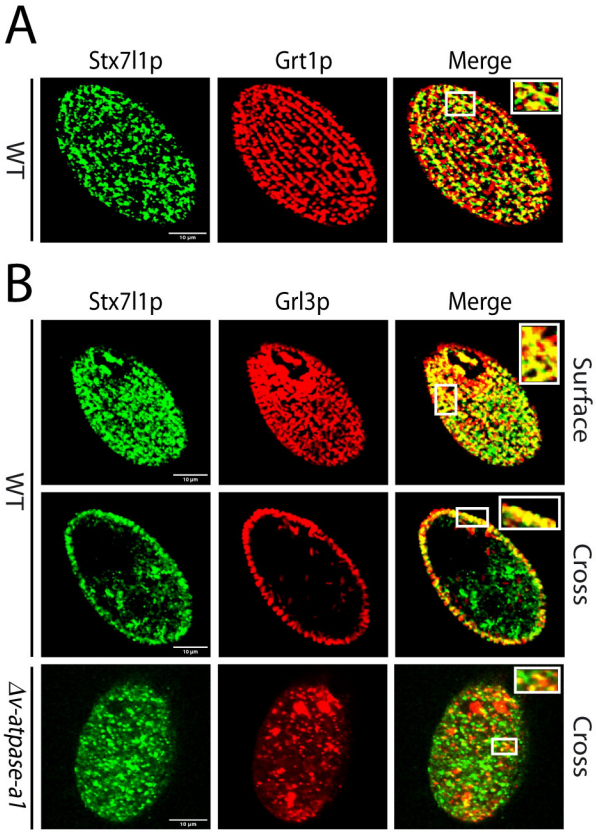
A
Stx7l1p
Grt1p
Merge
WT
B
Stx7l1p
Grl3p
Merge
WT
Surface
Cross
Δv-atpase-a1
Cross

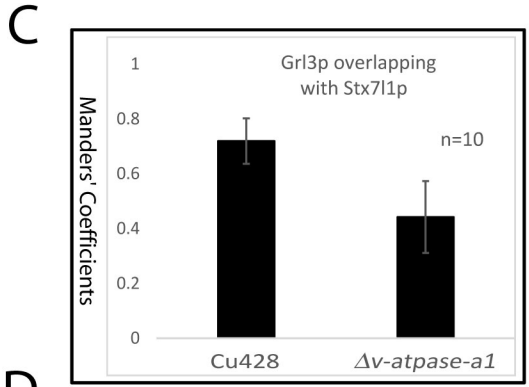
C
Grl3p overlapping
with Stx7l1p
Manders' Coefficients
1
0.8
0.6
0.4
0.2
0
n=10
Cu428
Δv-atpase-a1

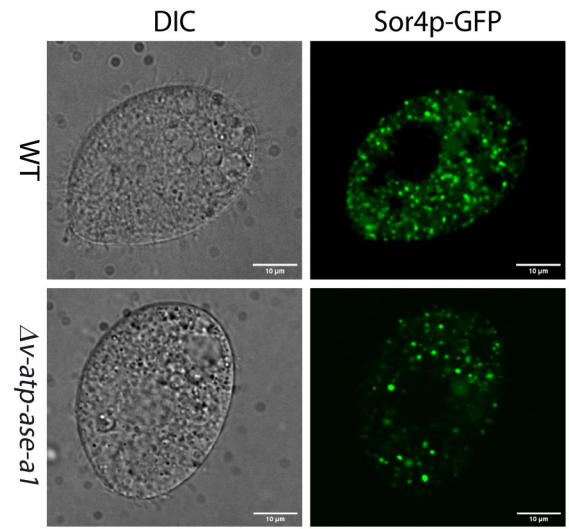
D
DIC
Sor4p-GFP
WT
Δv-atp-ase-a1